Journal Pre-proof



Deciphering interventional dynamical causality from non-intervention complex systems

Jifan Shi, Yang Li, Juan Zhao, Siyang Leng, Rui Bao, Kazuyuki Aihara, Luonan Chen, Wei Lin

PII: S2666-6758(26)00105-0

DOI: https://doi.org/10.1016/j.xinn.2026.101358

Reference: XINN 101358

To appear in: *The Innovation*

Received Date: 11 October 2025

Revised Date: 25 March 2026

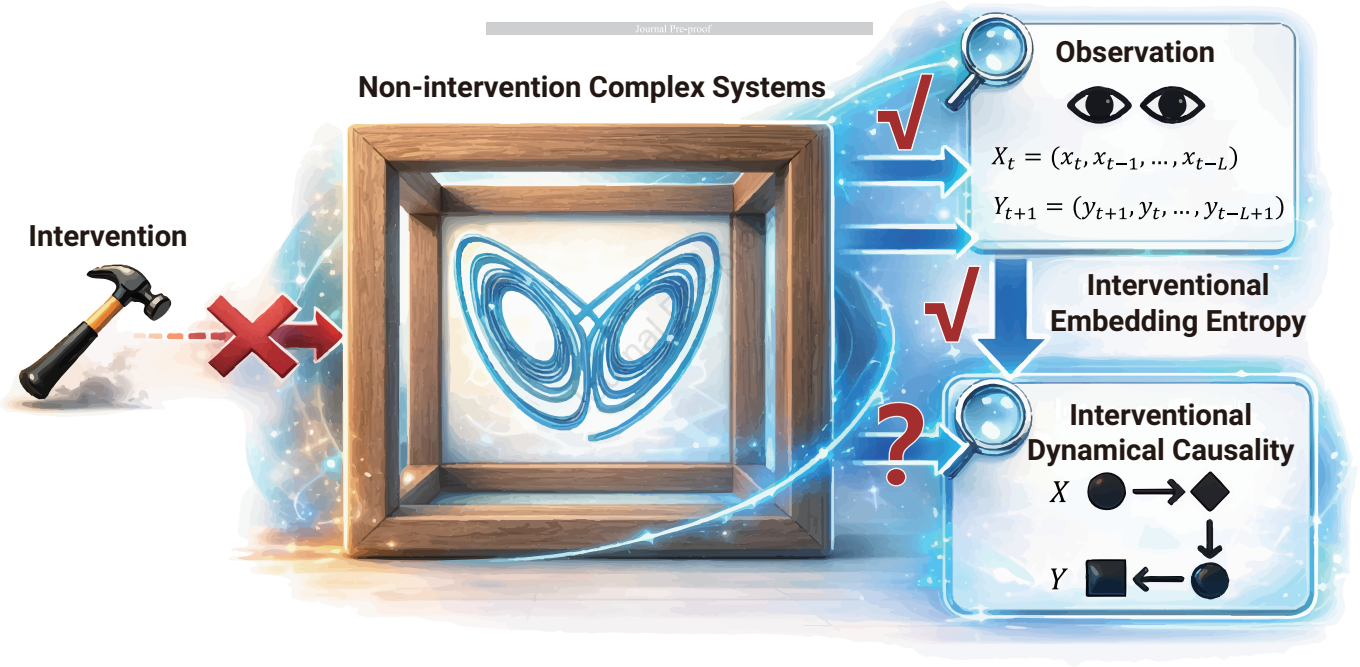
Accepted Date: 25 March 2026

Please cite this article as: Shi, J., Li, Y., Zhao, J., Leng, S., Bao, R., Aihara, K., Chen, L., Lin, W., Deciphering interventional dynamical causality from non-intervention complex systems, *The Innovation* (2026), doi: https://doi.org/10.1016/j.xinn.2026.101358.

This is a PDF of an article that has undergone enhancements after acceptance, such as the addition of a cover page and metadata, and formatting for readability. This version will undergo additional copyediting, typesetting and review before it is published in its final form. As such, this version is no longer the Accepted Manuscript, but it is not yet the definitive Version of Record; we are providing this early version to give early visibility of the article. Please note that Elsevier's sharing policy for the Published Journal Article applies to this version, see: https://www.elsevier.com/about/policies-and-standards/sharing#4-published-journal-article. Please also note that, during the production process, errors may be discovered which could affect the content, and all legal disclaimers that apply to the journal pertain.

© 2026 The Author(s). Published by Elsevier Inc. on behalf of Youth Innovation Co., Ltd.

Journal Pre-proof



Subject area: Computational Mathematics

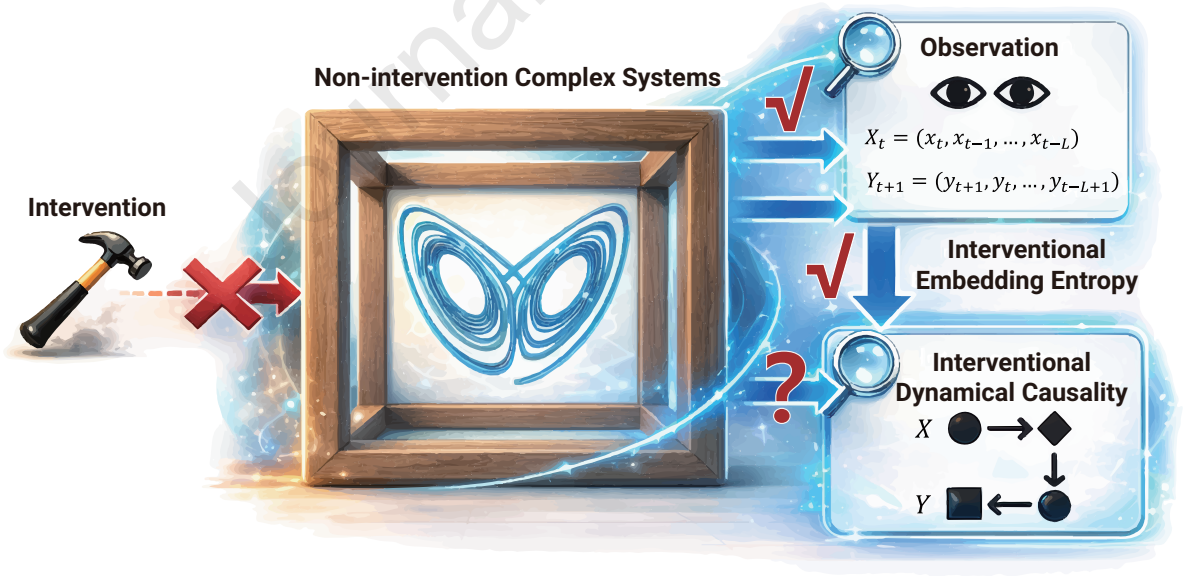
Deciphering interventional dynamical causality from non-intervention complex systems

Jifan Shi[1,*], Yang Li[2], Juan Zhao[3], Siyang Leng[1,4], Rui Bao[5], Kazuyuki Aihara[2,*], Luonan Chen[6,7,*], Wei Lin[1,*]

[1]Research Institute of Intelligent Complex Systems & CISOR, Fudan University, Shanghai 200433, China
[2]International Research Center for Neurointelligence, The University of Tokyo Institutes for Advanced Study, The University of Tokyo, Tokyo 113-0033, Japan
[3]School of Pharmacy, Shanghai University of Traditional Chinese Medicine, Shanghai 201203, China
[4]Institute of AI and Robotics, College of Intelligent Robotics and Advanced Manufacturing, Fudan University, Shanghai 200433, China
[5]Frontiers Science Center for Deep Ocean Multispheres and Earth System, Key Laboratory of Marine Chemistry Theory and Technology, and Innovation Center for Ocean Carbon Neutrality, Ocean University of China, Qingdao 266100, China
[6]School of Mathematical Sciences and School of AI, Shanghai Jiao Tong University, Shanghai 200240, China
[7]Key Laboratory of Systems Health Science of Zhejiang Province, School of Life Science, Hangzhou Institute for Advanced Study, University of Chinese Academy of Sciences, Chinese Academy of Sciences, Hangzhou 310024, China
*Correspondence: jfshi@fudan.edu.cn (J.S.); kaihara@g.ecc.u-tokyo.ac.jp (K.A.); lnchen@sjtu.edu.cn (L.C.); wlin@fudan.edu.cn (W.L.)

Journal Pre-proof

GRAPHICAL ABSTRACT



PUBLIC SUMMARY

- A theoretical framework for interventional dynamical causality is proposed.
- Dynamical systems theory is integrated with modern causal inference.

- The interventional embedding entropy (IEE) method quantifies causal strength directly from observational data.
- The IEE approach enables robust and effective causal detection across diverse non-intervention complex systems.

ABSTRACT

Detecting and quantifying causal influence is a focal topic in the fields of science, engineering, and interdisciplinary studies. However, causal studies on non-intervention systems attract much attention but remain extremely challenging. Delay-embedding technique provides a promising approach. In this study, we propose a framework named Interventional Dynamical Causality (IntDC) in contrast to the traditional Constructive Dynamical Causality (ConDC). ConDC, including Granger causality, transfer entropy and convergence of cross-mapping, measures the causality by constructing a dynamical model without considering interventions. A computational criterion, Interventional Embedding Entropy (IEE), is proposed to measure causal strengths in an interventional manner. IEE is an intervened causal information flow but in the delay-embedding space. Further, the IEE theoretically and numerically enables the deciphering of IntDC solely from observational (non-interventional) time-series data, without requiring any knowledge of dynamical models or real interventions in the considered system. In particular, IEE can be applied to rank causal effects according to their importance and construct causal networks from data. We conducted numerical experiments on Logistic dynamics, coupled-Hénon maps, and chaotic neural networks to demonstrate that IEE can find causal edges accurately, eliminate effects of confounding, and quantify causal strength robustly over traditional indices. We also applied IEE to real-world tasks, including estimating neural connectomes of *C. elegans*, detecting COVID-19 transmission networks in Japan, and investigating regulatory networks surrounding key circadian genes. IEE performed as an accurate and robust tool for causal analyses solely from the observational data. Both the IntDC framework and the IEE algorithm proposed in this study provide an approach to understanding causal influence in diverse non-intervention complex systems.

KEYWORDS

dynamical systems, causal influence, delay embedding, interventional embedding entropy, network reconstruction

INTRODUCTION

Directional or indirectional interactions among different components give rise to a variety of complex phenomena in nature and social society. The causality or the causal effect is one of the most attractive directional relations originating from the non-reversibility of time. Modeling, detecting, and quantifying causal influence from observational data are crucial for describing, interpreting, predicting, and even controlling complex systems.

Statisticians believe that causality is contained and obtainable in universal random variables regardless of the time label. Neyman-Rubin's potential outcome framework[1–3], the Wright's structural equation model[4,5] and the Pearl's causal diagram model[6,7] are the most famous statistical approaches, which have been proved to be of mathematical equivalence[8]. Especially, the instrumental variable method is widely applied in the study of causality among economics, environments, and other disciplines[9]. Statistical methods seek to discern binary causal relations among random variables on a directed acyclic graph, without relying on temporal data. However, in general complex dynamical systems, the causation must precede the effect, feedback is common, and the causal strength needs to be quantitatively measured. Time should play definitely a key role.

Dynamics-oriented researchers have proposed fruitful algorithms for measuring the observational causality from time series, commonly referred to as the dynamical causality[10]. The celebrated Granger causality (GC)[11,12] employs a linear model and uses improvement of predictability over time to illustrate the causality. Transfer entropy (TE)[13] generalizes GC to the nonlinear case by quantifying the prediction uncertainty through Shannon entropy. GC and TE rely on the separability assumption, namely that removing one variable from the system does not influence the others. Neither GC nor TE addresses the "non-separability" problem, in which removing a causal variable inevitably alters the dynamics of downstream variables. A systematic discussion of the separability issue can be found in recent

studies [10,14–16]. To measure causality in non-separable systems, numerous approaches have emerged in the last decade within the framework of delay embedding. These include convergence of cross mapping (CCM) [14,17], partial cross mapping (PCM) [15], continuity scaling [16], inverse continuity [18], topological expansion [19], joint distance distribution [20], embedding entropy (EE) [10] and other indices [21,22]. Besides, Runge et al. designed the PCMCI method to further remove "common drivers" by selecting parent nodes iteratively [23]. Friston et al. proposed the dynamical causal modeling (DCM), which is a Bayesian fitting from data with pre-selected models [24]. DCM was originally developed for modeling neural dynamics [25]. Krakovská et al. conducted a comparative analysis of six methods for detecting causality in bivariate systems [26].

Nonetheless, most indices designed for quantifying causality from time series primarily focus on estimating directional causal relationships at the constructive level, referred to as constructive dynamical causality (ConDC). Traditionally, to detect and quantify causality at the interventional level, which is termed interventional dynamical causality (IntDC) in this study, requires intelligent modulation and manipulation of the dynamical system. By allowing external intervention to the system and recording data under different perturbations, frameworks such as perturbation cascade inference (PCI) [27] and dynamical causal effect (DCE) [28,29] provide relevant computational schemes. To detect asymmetry information transfer in known two-dimensional dynamical systems, Liang and Kleeman proposed an analytic approach named Liang-Kleeman information flow [30–32], which serves as a prototype for IntDC. This method quantifies causality by freezing one variable as a parameter, and evaluating the resulting outcomes using the Frobenius-Perron operator. The Liang information flow has been further extended to multivariate, stochastic, and quantum systems [33–36]. However, due to ethical or practical limitations, many real systems should be analyzed without any external intervention. An essential problem is how to measure IntDC solely from the observational data but at the interventional level.

In this study, we propose the IntDC framework and introduce a criterion named Interventional Embedding Entropy (IEE), which aims to identify and quantify IntDC between variables solely from the observational time series. Actually, IEE is rigorously derived by the theory of the delay embedding. Numerical IEE does not require specific prior knowledge of dynamics, and additional perturbation to the system is also unnecessary. Compared to ConDC indices, such as GC, TE, and CCM, IEE designed for IntDC has the capability to rank the importance of causal effects and construct directional causal networks more effectively. We demonstrate numerical experiments on both simulated examples and real datasets, including estimating neural connectomes of *C. elegans*, evaluating COVID-19 transmission in Japan, and constructing regulatory networks surrounding key circadian genes.

METHODS

Constructive dynamical causality

The definition of ConDC for a complex system in the original time-series space is given as follows:

Definition 1 (Constructive dynamical causality, ConDC [10])**.** *For a complex dynamical system*

$$\boldsymbol{x}_{t+1} = \boldsymbol{f}(\boldsymbol{x}_t, \boldsymbol{x}_{t-1}, \ldots, \boldsymbol{x}_{t-p}) + \boldsymbol{\varepsilon}_t, \tag{1}$$

where $\boldsymbol{x} = (x^{(1)}, x^{(2)}, \ldots, x^{(n)})^T$ *represents the system with n components,* $\boldsymbol{f} = (f_1, f_2, \ldots, f_n)^T$ *is a vector function, p is referred to the memory time, and* $\boldsymbol{\varepsilon}_t$ *is an independent noise term, there exists ConDC from component* $x^{(j)}$ *to* $x^{(i)}$*, if* $\exists\, k \in \{0, 1, 2, \ldots, p\}$ *such that* $\partial f_i / \partial x^{(j)}_{t-k} \neq 0$ *for almost any t.*

For simplicity, we consider a discrete two-variable dynamical system as an example:

$$\begin{cases} x_{t+1} = g(x_t, x_{t-1}, \ldots, x_{t-p}, \varepsilon_{x,t}), \\ y_{t+1} = f(x_t, x_{t-1}, \ldots, x_{t-p}, y_t, y_{t-1}, \ldots, y_{t-p}, \varepsilon_{y,t}), \end{cases} \tag{2}$$

where x, y are two variables, p denotes the time step during which causality is considered, and $\varepsilon_{\cdot,t}$ stand for small noise terms. According to Definition 1, there exists ConDC from x to y since the evolving equation of y_{t+1} depends on the historical behavior of x, while there is no ConDC from y to x as the dynamics of x_{t+1} is independent of y. GC and TE measure the predictability of f in the original time-series space to quantify the ConDC from x to y through linear regression and entropy uncertainty, respectively (Figure **1**(B)). The causal strength of GC/TE is based on the

Journal Pre-proof

assumption of separability, which means that removing x from the system does not influence the observed data of y. However, in general coupled systems, the separability is not satisfied, as removing one variable changes the values of affected ones [14–16].

To address the challenge of detecting ConDC in universal non-separable systems, various approaches from the delay-embedding space have been proposed. In the delay-embedding framework, the bivariate system Eq. (2) is assumed to evolve into an attractive manifold with an inner dimension d. Let the time-delayed vectors of x and y be

$$\boldsymbol{X}_t = (x_t, x_{t-1}, \ldots, x_{t-L})^T \in \mathcal{M}_X \subseteq \mathbb{R}^{L+1}, \tag{3}$$

and

$$\boldsymbol{Y}_{t+1} = (y_{t+1}, y_t, y_{t-1}, \ldots, y_{t-L+1})^T \in \mathcal{M}_Y \subseteq \mathbb{R}^{L+1}, \tag{4}$$

where L is the time-delayed length, $\mathcal{M}_X$ and $\mathcal{M}_Y$ represent the manifolds formed by $\boldsymbol{X}_t$ and $\boldsymbol{Y}_t$, respectively. According to the seminal stochastic version of Takens' embedding theorem [37–40], we can obtain the following theorem:

Theorem 1 (ConDC in delay-embedding space)**.** *If x is the ConDC of y in dynamics Eq.* (2)*, and $\boldsymbol{X}_t$, $\boldsymbol{Y}_t$ are the time-delayed vectors, respectively, then there exists a smooth projection operator $\boldsymbol{F}$ in generic sense such that*

$$\boldsymbol{X}_t = \boldsymbol{F}(\boldsymbol{Y}_{t+1}), \tag{5}$$

when the time-delayed length satisfies $L \geqslant 2d$, where d is the inner dimension of the attractive manifold.

The detailed derivation can be referred to the Supplementary Text. The "generic sense" means that a smooth projection exists for a dense and open set of all possible time-delayed ways [37,38]. Equation (5) shows that the causal variable $\boldsymbol{X}_t \in \mathcal{M}_X$ can be reconstructed by the effect variable $\boldsymbol{Y}_{t+1} \in \mathcal{M}_Y$. However, as $\boldsymbol{F}$ is not reversible in generic sense, we can not determine $\boldsymbol{Y}_{t+1}$ only by the information from $\boldsymbol{X}_t$. According to Theorem 1, the causal dependence in f between x and y is transformed into the reconstructability of $\boldsymbol{F}$ (Figure **1**(D)). Theorem1, established for the dynamical system in Eq. (2), can be generalized to multi-variable systems as described in Eq. (1), allowing for feedback interactions between different variables. Instead of fitting a model by removing the causal variable as in GC and TE, detecting the existence and quantifying the continuity characteristics of $\boldsymbol{F}$ in the delay-embedding space can be adequate for causal identification, especially for universal non-separable systems. Related algorithms include CCM, PCM, and EE.

Figures **1**(A), (B) and (D) summarize dynamical causality at the constructive level, where the ConDC from variable x to y is estimated only from the historical observed time series. But fitting Eq. (2) or Eq. (5) from data is criticized as mere association or prediction [41,42].

Interventional dynamical causality

The detection of hidden essential-level causality necessitates intervention or manipulation to the system [8,27,43,44]. In this study, we propose the definition of IntDC for a complex system in the original time-series space as the following:

Definition 2 (Interventional dynamical causality, IntDC)**.** *For a complex dynamical system Eq.* (1)*, one component $x^{(j)}$ is the IntDC of another component $x^{(i)}$, if $\exists\, k \in \{0, 1, 2, \ldots, p\}$ such that $\delta x^{(i)}_{t+1} = \tilde{x}^{(i)}_{t+1} - x^{(i)}_{t+1}$ depends on $\delta x^{(j)}_{t-k} = \tilde{x}^{(j)}_{t-k} - x^{(j)}_{t-k}$ for almost any t, where $\tilde{x}^{(j)}_{t-k}$ is the intervened dynamics of $x^{(j)}$, and $\tilde{x}^{(i)}_{t+1}$ is the dynamics of affected $x^{(i)}$ after the intervention on $x^{(j)}$.*

The intervention $\delta x^{(j)}_{t-k}$ can be either a pulse stimulation or persistent disturbances to the system. Figure **1**(C) illustrates the IntDC in the time-series space for the simplified bivariate system Eq. (2), involving variables x and y. To measure the IntDC, data before and after the intervention, i.e. (x_t, y_t) and $(\tilde{x}_t, \tilde{y}_t)$, are typically required, as in PCI and DCE. PCI measures the distances of every node in the network from each perturbed node to reconstruct the directed causal network [27]. DCE classified causal coupling into four situations based on the type of effects (stationary statistic change, phase orbit change) and the type of interventions (state space interventions, parametric interventions) [28]. These conventional algorithms rely on reproducible dynamics or data availability under different settings.

To address challenges of causal inference in widespread non-intervention, non-linear and non-separable systems, we turn to the study of intervened dynamics of Eq. (5) in the delay-embedding space. Denote $\delta \boldsymbol{X}_t = \widetilde{\boldsymbol{X}}_t - \boldsymbol{X}_t$ and $\delta \boldsymbol{Y}_{t+1} = \widetilde{\boldsymbol{Y}}_{t+1} - \boldsymbol{Y}_{t+1}$, where $\widetilde{\boldsymbol{X}}_t$ and $\widetilde{\boldsymbol{Y}}_{t+1}$ are the time-delayed vectors of x and y after the intervention, respectively. We can obtain the following theorem:

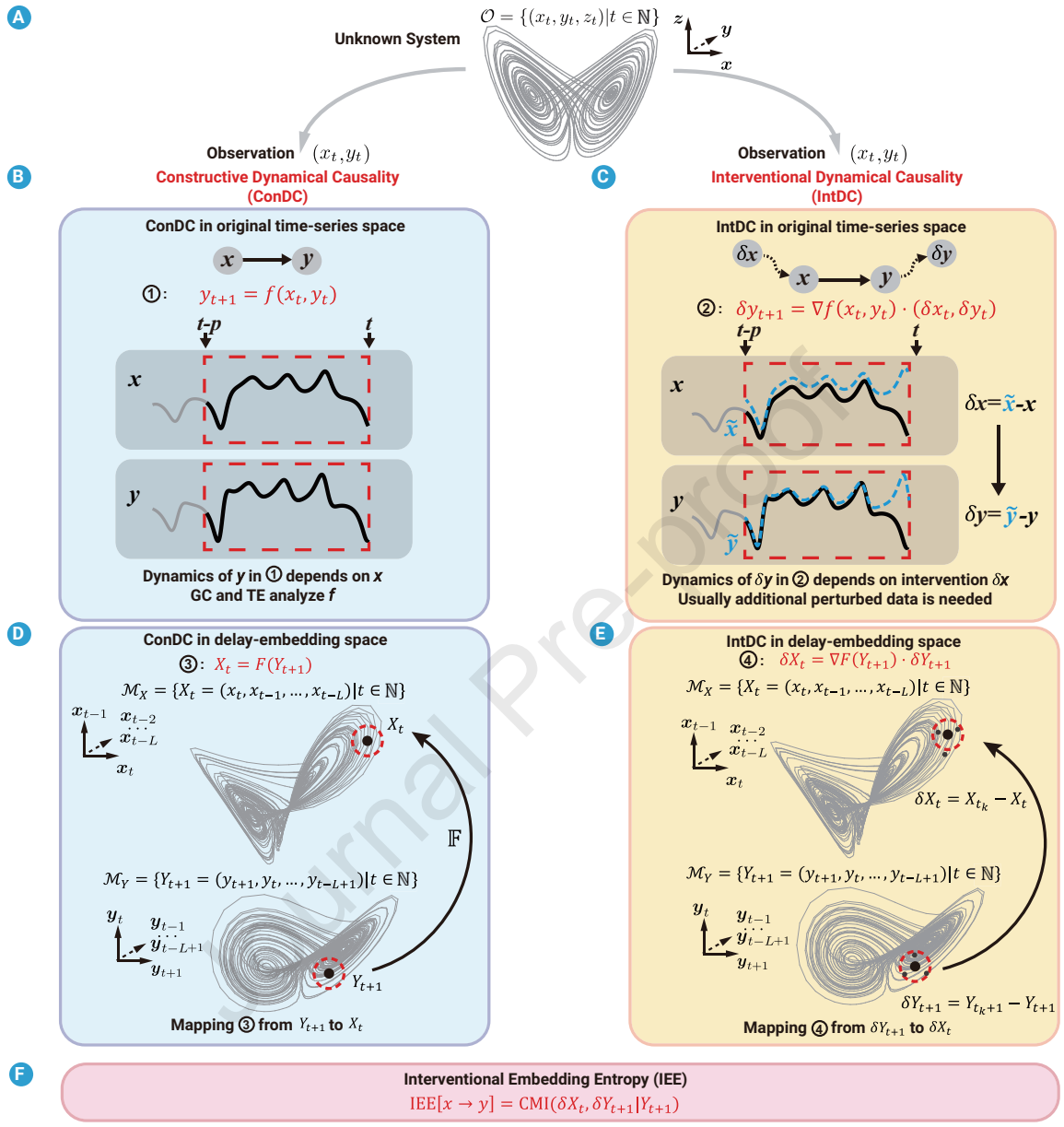


Figure 1. **Illustration for the constructive dynamical causality (ConDC) and interventional dynamical causality (IntDC)** (A) An illustrative example of a complex system where (x_t, y_t) are observed time series. The z_t stands for the other variable that is not the primary focus of analysis. (B) ConDC from x to y indicates that the dynamics of y depends on x. Algorithms such as Granger causality (GC) and transfer entropy (TE) infer the ConDC in the original time-series space. (C) IntDC from x to y indicates that the deviation of y, i.e. δy, depends on an intervention on x, i.e. δx. Usually additional data from a perturbed system $(\tilde{x}_t, \tilde{y}_t)$ is necessary for detecting IntDC in the original time-series space. The parameter p is the time lag after intervention occurs. (D) ConDC can be detected in the embedding space by cross mapping $\mathbb{F}$. The causal vector $\boldsymbol{X}_t$ can be reconstructed by the effect vector $\boldsymbol{Y}_{t+1}$. Parameter L is time delay used in the delay-embedding. (E) IntDC can be modeled in the embedding space. The interventional causal vector $\delta\boldsymbol{X}_t$ should be reconstructable by the effect vector $\delta\boldsymbol{Y}_{t+1}$ around $\boldsymbol{Y}_{t+1}$. In numerical computation, $\delta\boldsymbol{Y}_{t+1}$ is approximated by the distance from $\boldsymbol{Y}_{t+1}$ to its neighbors $\boldsymbol{Y}_{t_k+1}$, while $\delta\boldsymbol{X}_t$ is determined using $\boldsymbol{X}_{t_k}$ corresponding to the same time index t_k. (F) Interventional embedding entropy (IEE) measures the average information retention contained in $\delta\boldsymbol{Y}_{t+1}$ from $\delta\boldsymbol{X}_t$, quantifying the IntDC from variable x to y. Notably, IEE does not require additional perturbations to the system and can be inferred from observational data solely.

Theorem 2 (IntDC in delay-embedding space)**.** *If x is the IntDC of y in dynamics Eq.* (2)*, and $\boldsymbol{X}_t, \boldsymbol{Y}_t$ are the time-*

Journal Pre-proof

delayed vectors, respectively, then there exists a smooth projection operator $\boldsymbol{F}$ *in generic sense such that*

$$\delta \boldsymbol{X}_t = \nabla_{\boldsymbol{Y}} \boldsymbol{F}(\boldsymbol{Y}_{t+1}) \cdot \delta \boldsymbol{Y}_{t+1}, \tag{6}$$

when the time-delayed length satisfies $L \geq 2d$ *and the intervention is sufficiently small, where* d *is the inner dimension of the attractive manifold.*

Theorem 2 is directly deduced by Theorem 1. However, Eq. (6) provides insights on the causality under intervention. It indicates that $\delta \boldsymbol{Y}_{t+1}$ contains complete information of $\delta \boldsymbol{X}_t$ in the neighborhood of $\boldsymbol{Y}_{t+1}$ and can reconstruct $\delta \boldsymbol{X}_t$, if there exists IntDC from the causal variable x to the effect variable y (Figure **1**(E)). The conclusion in Eq. (6) of Theorem 2, derived from the dynamics in Eq. (2), remains valid for any pair of components exhibiting IntDC in the multi-variable system of Eq. (1), and feedback between different components is permitted. Figures **1**(A), (C), and (E) give an overview of the IntDC framework.

Regarding the relationship between Definition 1 and Definition 2, we claim that, in theory, the existence of IntDC between two variables is a sufficient condition for the existence of ConDC. IntDC can be interpreted as a dependence captured by the first-order differential form of ConDC in Eq. (1). However, in practical situations, direct numerical estimation of ConDC suffers from false positives, particularly in the presence of confounders (see section 3.2).

Interventional embedding entropy

We introduce the IEE criterion, specifically designed for quantifying IntDC solely from the observational data in the delay-embedding space.

Definition 3 (Interventional embedding entropy, IEE)**.** *The IEE criterion is proposed to measure the average information retention or reconstructability from the effect* $\delta \boldsymbol{Y}_{t+1}$ *to the causation* $\delta \boldsymbol{X}_t$*, formulated as*

$$\mathrm{IEE}[x \to y] := \mathrm{CMI}(\delta \boldsymbol{X}_t, \delta \boldsymbol{Y}_{t+1} | \boldsymbol{Y}_{t+1}). \tag{7}$$

In Eq. (7), CMI is the conditional mutual information[45], i.e.

$$\mathrm{CMI}(\boldsymbol{x}, \boldsymbol{y}|\boldsymbol{z}) = \iiint p(\boldsymbol{x}, \boldsymbol{y}, \boldsymbol{z}) \log \frac{p(\boldsymbol{x}, \boldsymbol{y}|\boldsymbol{z})}{p(\boldsymbol{x}|\boldsymbol{z}) p(\boldsymbol{y}|\boldsymbol{z})} \, \mathrm{d}\boldsymbol{x} \, \mathrm{d}\boldsymbol{y} \, \mathrm{d}\boldsymbol{z}. \tag{8}$$

IEE provides is a quantitative measure of causal strength that is comparable across different edges within the same dynamical system. When dealing with data, the $\delta \boldsymbol{Y}_{t+1}$ is estimated by the distance from $\boldsymbol{Y}_{t+1}$ to its neighbored points $\boldsymbol{Y}_{t_k+1}$ in the embedding space, and $\delta \boldsymbol{X}_t$ is calculated by $\boldsymbol{X}_{t_k}$ with the same time label t_k (Figs. **1**(E) and (F)). Thus, Eq. (7) can be numerically approximated only from the observational data, especially for non-intervention systems. Table **1** presents the numerical algorithm for computing IEE, whose detailed descriptions and computational procedures are provided in the Supplementary Text.

Table 1. Algorithm: Interventional Embedding Entropy (IEE).

1. Given observed time series $\{x_{t_n} \| t_n \geq 0\}, \{y_{t_n} \| t_n \geq 0\}$.
2. Construct time-delayed vectors $\boldsymbol{X}_{t_n}$ and $\boldsymbol{Y}_{t_n+1}$ by Eqs. (3)-(4).
3. Get K nearest neighbors $\boldsymbol{Y}_{t_k+1}$ around $\boldsymbol{Y}_{t_n+1}$, $k = 1, 2, \ldots, K$.
4. Sample $\delta \boldsymbol{Y}_{t_n+1}$ condition on $\boldsymbol{Y}_{t_n+1}$ as $\boldsymbol{Y}_{t_k+1} - \boldsymbol{Y}_{t_n}$.
5. Sample $\delta \boldsymbol{X}_{t_n}$ condition on $\boldsymbol{Y}_{t_n+1}$ as $\boldsymbol{X}_{t_k} - \boldsymbol{X}_{t_n}$ with the same time labels t_k.
6. Calculate Eq. (7) around $\boldsymbol{Y}_{t_n+1}$ and average over n samples to approximate $\mathrm{IEE}[x \to y]$.

Connections with statistical causal models and assumptions of ConDC/IntDC

The concept of dynamical causality in Eq. (1) develops from traditional structural causal models, which typically studies structure equations of the form $Y = f(X, \varepsilon, \theta)$, where X and Y are random variable, f is a function parameterized by θ, and ε represents noise or residue terms. The framework of ConDC has been systematically studied

Journal Pre-proof

with three key generalizations beyond classical structural equation modeling [10]: (i) Temporal information is fully considered by dynamical systems, ensuring that causes precede effects in time; (ii) Feedback or causal loops between variables are permitted under the consideration of time delays, relaxing the restriction of directed acyclic graphs (DAGs); (iii) Quantitative measures of causal strength are provided beyond qualitative identification, enabling direct comparisons of causality between different variables. The IntDC proposed in the study further integrates the concept of interventions and potential outcomes within the dynamical framework [8]. IntDC aims to quantify causal strengths at the interventional level directly from observational data (without the need for additional interventions to the system, which are often impractical or infeasible in real-world datasets).

The following assumptions (A1)-(A8) clarify key connections between dynamical causality and statistical causal inference:

(A1) Temporal Order assumption: Causal information is embedded in time-series data and causes must precede their effects;

(A2) Causal Sufficiency (Unconfoundedness) assumption: All common drivers (confounders) are observed such that the causal graph accurately represents relationships among the observed variables;

(A3) Causal Markov assumption: Each variable x_i is independent of its nondescendants given its direct causes (parents);

(A4) Faithfulness assumption: The causal graph structure can represent the conditional independence contained in the joint probability density;

(A5) Stationarity assumption: The dynamical system evolves into a stable attractive manifold, allowing stable causal relations to be measured from observational data;

(A6) Intervention Ignorability assumption: Given the system dynamics Eq. (1), initial conditions $\boldsymbol{x}_0$ and noise $\boldsymbol{\varepsilon}_t$, the intervention on variable $x^{(j)}$ at time $t-k$ is independent of the potential outcome of $x^{(i)}$ at time $t+1$, i.e. $x^{(i)}_{t+1} \perp\!\!\!\perp \delta x^{(j)}_{t-k} | (\boldsymbol{f}, \boldsymbol{x}_0, \boldsymbol{\varepsilon}_t)$ for $k = 0, 1, 2, \ldots, p$;

(A7) Stable Infinitesimal Intervention assumption: The average information retention from $x^{(j)}$ to $x^{(i)}$ in dynamics Eq. (1) remains stable under sufficiently small interventions $\delta x^{(j)}$;

(A8) Consistency assumption: The outcome $\tilde{x}^{(i)}_{t+1}$ in Eq. (1) can be precisely determined under known dynamics $(\boldsymbol{f}, \boldsymbol{x}_0, \boldsymbol{\varepsilon}_t)$ and a fixed intervention $\delta x^{(j)}_{t-k}$.

In practice, (A2) can be relaxed if the primary goal is to quantify the total causal strength (including both direct and indirect causality) between observed variables. In the Results section, we demonstrate that the IEE criterion is capable of mitigating the impact of confounding variables, thereby providing robust causal estimates even when some confounders are unobserved. Some of these assumptions for causal discovery from observational time-series data have also been discussed by Runge et al. [23,46]

GC, TE, and CCM are all criteria for ConDC, which estimate causal strengths by fitting constructive dynamical models (i.e. Eq. (2) in the time-series space or Eq. (5) in the delay-embedding space). GC employs linear vector regression to fit $\boldsymbol{f}$ in Eq. (2). TE extends GC to nonlinear cases by quantifying information transfer between variables. CCM constructs a local-linear cross-mapping $\boldsymbol{F}$ in Eq. (5) by the time-delayed embedding to capture causality. For a detailed comparison of these ConDC methods, readers are referred to Table 1 in Shi et al. [10] IEE captures causality at the interventional level, whereas GC, TE, and CCM are restricted to association level causality. Moreover, IEE as one measure for IntDC can effectively avoid confounding effects in structures such as $x \leftarrow z \rightarrow y$ (see section 3.2).

RESULTS AND DISCUSSIONS

IEE captures the numerical behavior of causality in Logistic systems robustly

To assess the numerical performance of measuring IntDC, we first applied the IEE algorithm on the following two-node Logistic dynamics

$$\begin{cases} x_{t+1} = 3.7[(1-\beta_{yx})x_t(1-x_t) + \beta_{yx}y_t(1-y_t)] + \varepsilon_{x,t}, \\ y_{t+1} = 3.7y_t[1-(1-\beta_{xy})y_t - \beta_{xy}x_t] + \varepsilon_{y,t}, \end{cases} \tag{9}$$

where $\varepsilon_{\cdot,t}$ represents independent Gaussian noises, and parameters β_{xy} and β_{yx} modulate the IntDC strength from x to y and from y to x, respectively (see further details in SM).

IEE can capture the numerical behavior of IntDC in the two-node Logistic system. When we set $\beta_{xy} \equiv 0$ and let β_{yx} increase from 0 to 0.3. we observed a monotonic increase in IEE[$y \to x$] (the red line with squares in Figure **2**(A)), while IEE[$x \to y$] remained around zero (the blue line with dots in Figure **2**(A)). When we set $\beta_{xy} \equiv 0.1$ and let β_{yx} increase from 0 to 0.3, IEE[$y \to x$] exhibited a monotonic increase (the red line with squares in Figure **2**(B)), while IEE[$x \to y$] stayed above zero (the blue line with dots in Figure **2**(B)). The gray dashed lines in Figs. **2**(A-B) represent 0.01 for reference. A detailed comparison with GC, TE and CCM is presented in figs.S1 and S2. The mean values and standard deviations of the indices over 100 simulation runs are provided in tables S1-S4. Fig. S1(b) and fig. S2(b) indicate that GC exhibited non-monotonic behavior. TE[$y \to x$] demonstrated a decreasing trend when β_{yx} increased, specifically for $\beta_{yx} \in (0, 0.02]$ in fig. S1(c)/table S1 and $\beta_{yx} \in (0, 0.03]$ in fig. S2(c)/table S3, which may lead to false-negative issues (ignorance of existence causality). CCM[$x \to y$] remained significantly different from zero even when $\beta_{xy} = 0$ (in the range $\beta_{yx} \in [0.15, 0.3]$ in fig. S1(d)/table S2). CCM[$y \to x$] was also significantly different from zero when $\beta_{yx} = 0$ (with $\beta_{xy} = 0.1$ in fig. S2(d)/table S3). These results suggest that CCM may suffer from the false-positive problem (incorrect identification of non-existence causality).

Within suitable parameter ranges, IEE demonstrates stability and robustness. We validated the robustness of the IEE algorithm under various conditions, including different delayed lags L, the numbers of nearest neighbors K, lengths of time series N, and noise standard deviations σ. The causal strengths measured by IEE exhibited a consistent descending trend as β_{yx} decreased from 0.15 to 0.05 through $0.125, 0.1, 0.075$, as expected (Figs. **2**(D-G)). These results support that IEE reliably preserves the correct ranking of causal strengths across different parameter settings with relatively stable variance.

IEE eliminates the influence of confounding variables

IEE remains applicable and accurate even in presence of confounding variables. We simulated a three-node Logistic dynamics (x_t, y_t, z_t), where z acted as a confounder (see details in SM). There were consistently non-zero causal effects from z to x and from z to y, while β_{xy} adjusted the causal strength from x to y (Figure **2**(C)). When $\beta_{xy} = 0$, IEE[$x \to y$] was almost zero and significantly different from IEE[$z \to x$] and IEE[$z \to y$] (Figure **2**(C)); but conventional ConDC indices such as GC/TE/CCM produced false-positive causality from x to y due to the presence of confounder z (fig. S3). According to the IntDC framework, an intervention on x (i.e. δx) will not induce an indirect change in y (i.e. δy) through z; in other words, there is no intervention-induced pathway through $x \leftarrow z \to y$. However, traditional ConDC indices by fitting dynamical models may falsely infer an association between x and y due to the influence of the confounder z. IEE, specially designed for measuring IntDC, remained unaffected by the confounder z and yielded accurate results.

IEE enables causal network reconstruction with quantification of causal strengths

IEE has the capability to reconstruct the causal network structure and rank the causal influence between nodes in complex networks at the interventional level. We used a 10-node coupled Hénon maps as an example, where each node serves as the dynamical cause to its subsequent node (Figure **3**(A)). Further details regarding the dynamics can be found in SM.

To verify the effectiveness of IEE in reconstructing causal networks, we calculated the Area Under Curve (AUC) values based on multiple simulated time series. The AUC value (mean ± standard deviation) of IEE was 0.871 ± 0.008, significantly higher than conventional ConDC indices, such as GC with 0.707 ± 0.069, TE with 0.816 ± 0.018, and CCM with 0.837 ± 0.012 (boxplots in Figure **3**(B)). The AUCs of IEE exhibited both a higher mean and a lower variance relative to other approaches. Additionally, receiver operating characteristic (ROC) curves for the four indices were presented in fig. S4.

To show the capability for ranking the importance of causal influences, we conducted two tests. We first calculated the IEE from Node 1 to the other nine nodes. Consistently with the actual scenario, IEE displayed sequential decrease in IntDC originating from Node 1 across Nodes 2 to 10 (Figure **3**(C)). Then, we measured the IEE received by Node 7 from the other nine nodes. As expected, Nodes 1-6 exhibited ascending causal strengths on Node 7, whereas Nodes 8-10 had little influence on Node 7 (Figure **3**(D)). IEE accurately discerned the IntDCs, with Node 6 showing the strongest value. A comparison showed that GC and TE failed to rank the influence from Node 1 accurately in the first test (fig. S5), while CCM suffered from the false-positive causal detection from Node 8 to Node 7 in the second test (fig. S6).

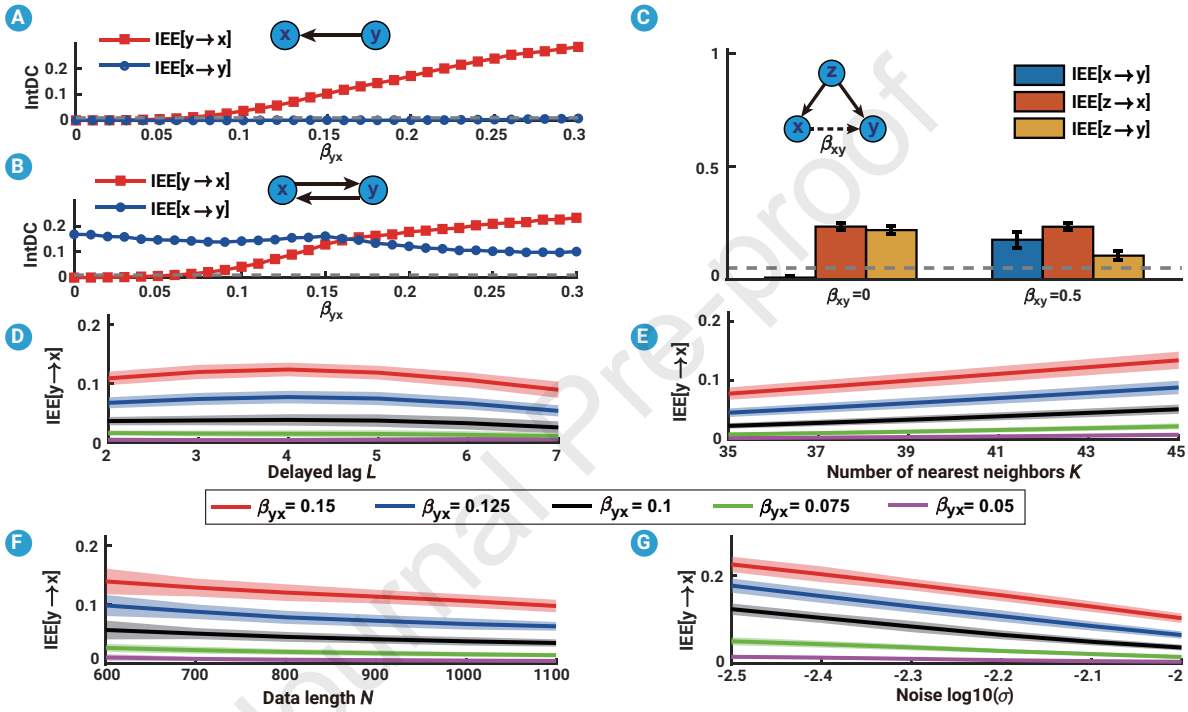


Figure 2. **Performance of IEE on Logistic systems** (A) and (B) used the two-node Logistic system. The β_{xy} and β_{yx} control the coupling coefficients from x to y and from y to x, respectively. (A) shows the mean values of IEE when $\beta_{xy} = 0$ and β_{yx} ranges from 0 to 0.3 over 100 simulations. IEE[$y \to x$] (the red line with squares) increases monotonically, while IEE[$x \to y$] (the blue line with dots) stays around zero. (B) is under $\beta_{xy} = 0.1$, in which IEE[$x \to y$] (the blue line with dots) is significantly positive. The gray dashed lines in (A) and (B) represent the constant 0.01 as reference. (C) shows the performance of IEE in the three-node Logistic system, where z acts as a confounding variable. When $\beta_{xy} = 0$, IEE[$x \to y$] is almost zero correctly. IEE designed for measuring IntDC is not affected by confounders, which usually leads to false positives in ConDC. The results for $\beta_{xy} = 0.5$ is shown for a comparison. The gray dashed line is 0.05 for reference. (D-G) demonstrate the robustness of IEE under different delayed lags L, the numbers of nearest neighbors K, data lengths N, and noise standard deviations σ in the two-node logistic system, respectively. The parameter $\beta_{xy} \equiv 0$, and β_{yx} takes values of 0.15 (red), 0.125 (blue), 0.1 (black), 0.075 (green), and 0.05 (magenta). Lines denote mean values under 50 simulations, and shaded areas represent the standard deviation. IEE consistently preserves the correct ranking of IntDC across various settings, with relatively stable variance.

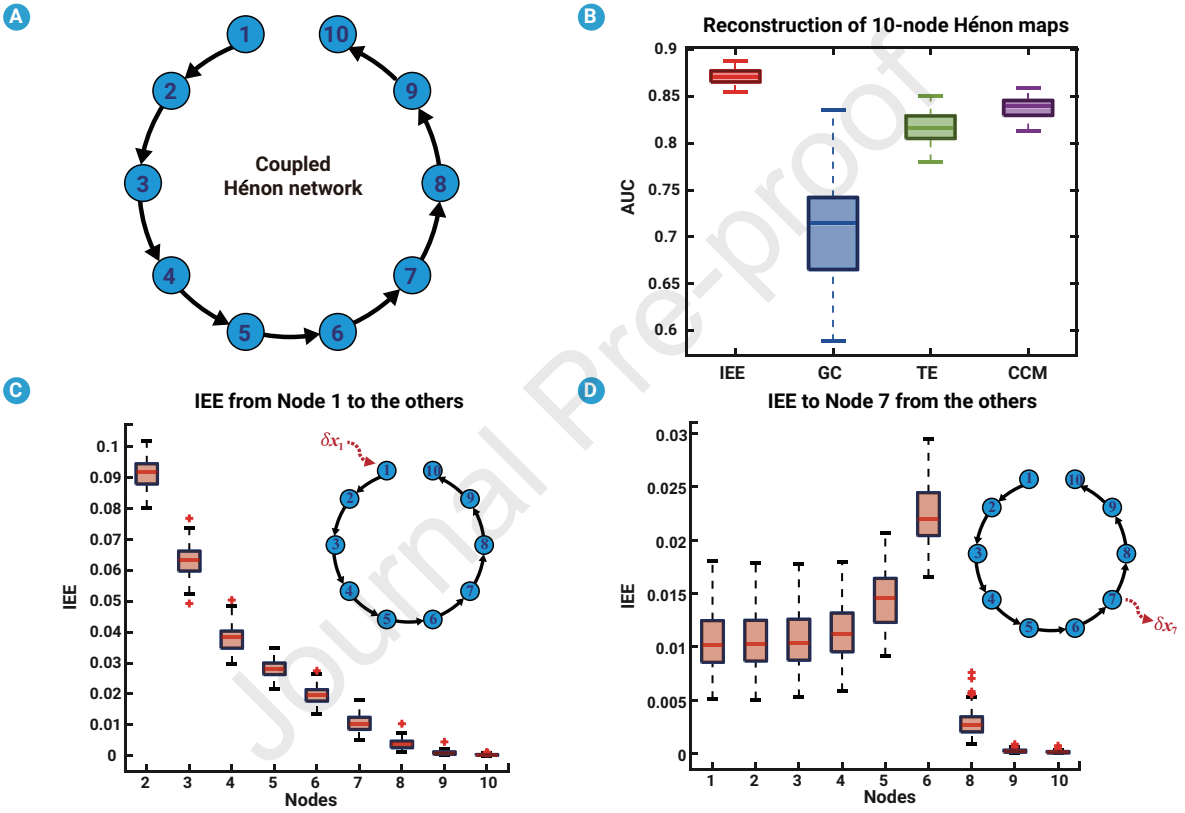


Figure 3. **Performance of IEE on the 10-node coupled Hénon-map dynamics** (A) illustrates the network structure of the dynamics. There are directed causality from each node to its subsequent node. (B) presents a boxplot of the Area Under Curve (AUC) values for the network reconstruction. IEE (0.871 ± 0.008) outperforms GC (0.707 ± 0.069), TE (0.816 ± 0.018), and CCM (0.837 ± 0.012) significantly in accuracy and stability. (C) demonstrates the IEE from Node 1 to the other nine nodes, while (D) shows the IEE received by Node 7 from the other nodes. IEE accurately captures the interventional information flow and IntDC in the cascade topological network.

Journal Pre-proof

IEE quantifies IntDC without requiring additional experimental interventions

IEE is specifically designed for calculating IntDC solely from observed time-series data without requiring additional perturbations to the system. To validate its accuracy, we conducted a comparison against true perturbed deviations using chaotic neural networks (chNNs) as a model system[47,48].

The chNN comprises an output variable $\boldsymbol{x} = (x_1, x_2, \ldots, x_{N_{\text{node}}})^T$ and two internal variables, with N_{node} representing the number of neurons in the network. We chose $N_{\text{node}} = 10$ in simulations. Details on the dynamics can be found in SM. We denoted the observed time-series data from the stationary system without intervention as $\boldsymbol{x}_{\text{obs}}$. When the neuron i was removed (set as a constant zero), the perturbed data were denoted as $\boldsymbol{x}^{(i)}_{\text{per}}$. Removing one node was taken as an intervention to the system. The stationary probability density functions of the jth neuron before and after the intervention were represented by $p_j(\boldsymbol{x}_{\text{obs}})$ and $p_j(\boldsymbol{x}^{(i)}_{\text{per}})$, respectively. We used the Kullback-Leibler divergence (KLD), i.e.

$$\begin{aligned} D_{ij} &\triangleq \text{KLD}[p_j(\boldsymbol{x}_{\text{obs}}) \| p_j(\boldsymbol{x}^{(i)}_{\text{per}})] \\ &= \iint p_j(\boldsymbol{x}_{\text{obs}}) \log \frac{p_j(\boldsymbol{x}_{\text{obs}})}{p_j(\boldsymbol{x}^{(i)}_{\text{per}})} \, \mathrm{d}\boldsymbol{x}_{\text{obs}} \, \mathrm{d}\boldsymbol{x}^{(i)}_{\text{per}}, \end{aligned} \tag{10}$$

to quantify the true influence of the intervention, i.e. ground truth of the IntDC, from i to j. By conducting 100 randomly simulated chNNs with interventions (in each simulation, one node is removed from each chNN with N_{node} nodes), we recorded 1000 KLD values and compared them with the results of IEE (calculated from $\boldsymbol{x}_{\text{obs}}$ solely). We observed that IEE$[x_i \to x_j]$ exhibited a positive linear correlation with the KLD D_{ij} (with $R^2 = 0.869$) in Figure **4**(A), where gray dots are the 1000 samples of causal edges between neurons and the red line stands for the linear regression. Results for GC (with $R^2 = 0.572$), TE (with $R^2 = 0.912$), and CCM (with $R^2 = 0.622$) indicated that GC and CCM could not linearly reflect KLD (Figs. **4**(B-D)). Furthermore, we drew the violin plots of cosine similarity S_c (see SM) between KLD and the four causal indices on 100 chNNs (Figure **4**(E)). IEE (0.904 ± 0.024) had the highest mean similarity with KLD, compared to GC (0.711 ± 0.076), TE (0.888 ± 0.022), and CCM (0.687 ± 0.033). In addition, we calculated the rank-based correlation coefficient Kendall's tau. CCM ($\rho_\tau^{\text{CCM}} = 0.457$) showed the strongest rank-based correlation with KLD, compared with IEE ($\rho_\tau^{\text{IEE}} = 0.383$), GC ($\rho_\tau^{\text{GC}} = 0.269$), and TE ($\rho_\tau^{\text{TE}} = 0.379$). These results indicate that IEE can accurately quantify IntDC from observational data $\boldsymbol{x}_{\text{obs}}$ alone and reflect KLD in a linear manner, alleviating the need for additional interventions to the dynamics.

Application of IEE in inferring neural connectomes of *C. elegans*

We applied the IEE criterion to infer the neural connectomes of *Caenorhabditis elegans* (*C. elegans*), a model organism known for its comprehensively studied nervous system[49]. Calcium fluorescence imaging time series data from 31 neurons with specific functions of a freely moving *C. elegans* were collected from Kato et al.[50] (see Figs. **5**(A-B) and fig. S7). The cosine similarity between different neurons were calculated and the neurons were clustered into 7 clusters after data preprocessing (see Figure **5**(C), Supplementary Text and table S5). We presented the ground truth of neural connectomes between clusters in a directed graph (Figure **5**(D)), which was detected by electron microscopy[49,51,52]. The IEE values between different clusters were calculated to infer the IntDC network. The ROC curve of IEE got a high AUC value 0.882 (Figure **5**(F)). By maximum Youden index, maximum concordance probability, and minimum distance to the point $(0, 1)$, IEE gave the same optimal operating point (OOP). At the OOP, IEE provided an inferred connectomic network with only 1 false positive and 4 false negatives (Figure **5**(E)). We also compared IEE with other ConDC indices, i.e. GC/TE/CCM, which revealed that IEE exhibited the highest AUC value, best OOP, largest similarity to the ground truth, lowest false positive at the OOP, and lowest false negative at the OOP (see Table **2**, figs. S8-S10, and table S6). Unidirectional edges are particularly sensitive to threshold selection and are prone to false-positive and false-negative inference. In the C. elegans network, there are 6 unidirectional edges among the 26 directed edges (edges $2 \to 3, 2 \to 4, 2 \to 5, 7 \to 4, 7 \to 5, 7 \to 6$ in Figure **5**(D)). CCM and IEE showed comparable performance for bidirectional edges, while IEE achieves the lowest error rate for unidirectional edges compared with other indices (Figure **5**, fig. S10, and Table S6).

Additionally, we inferred the connectomic network using the PCMCI algorithm with two approaches: the partial correlation (PCMCI-ParCorr) and CMI test (PCMCI-CMI). PCMCI used an independence test with the only parameter being the significance level α_{PC}. The false positive edges for PCMCI-ParCorr ($\alpha_{\text{PC}} = 0.05$) and PCMCI-CMI ($\alpha_{\text{PC}} =$

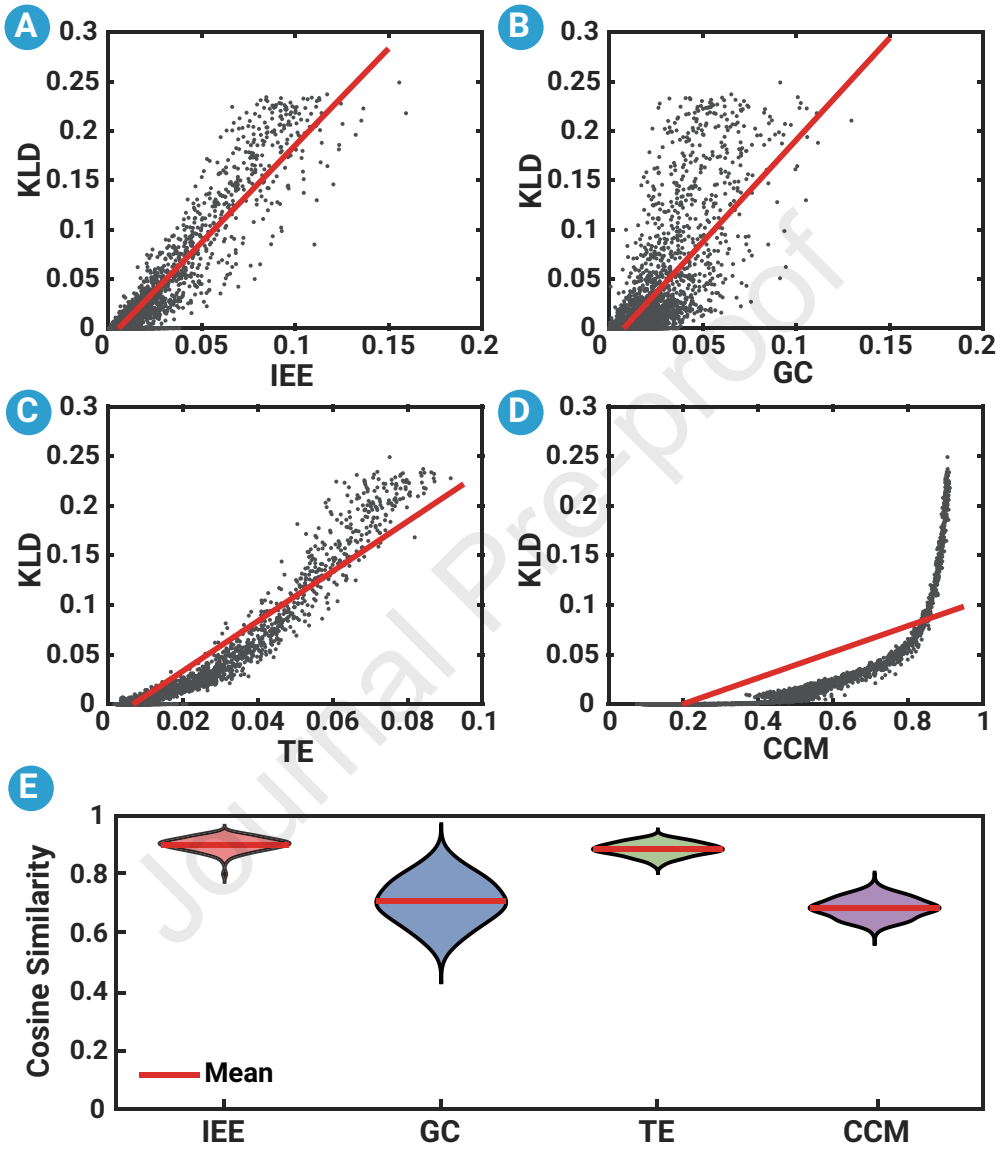


Figure 4. **The performance of IEE when measuring the influence of perturbations on the chaotic neural networks (chNNs)** The Kullback-Leibler divergence (KLD) is utilized to measure the true influence or IntDC between neurons. In (A-D) , 1000 samples for different perturbations on chNNs are represented by gray dots, along with the linear regressions (the red lines) between KLD and IEE/GC/TE/CCM, respectively. (E) displays the violin plots of cosine similarity between KLD and IEE/GC/TE/CCM. The mean values and standard deviations of the cosine similarity are IEE (0.904 ± 0.024), GC (0.711 ± 0.076), TE (0.888 ± 0.022), and CCM (0.687 ± 0.033). IEE can linearly reflect the KLD with high similarity, indicating its effectiveness in accurately quantifying IntDC without additional perturbed data on chNNs.

0.01) are 5 and 6, respectively. Both approaches have 4 false negative edges. A detailed description of the procedure and results can be found in the Supplementary Text, figs. S10(e-f) and table S6.

These findings demonstrate the efficacy of IEE in reconstructing the neural connectomes of *C. elegans*.

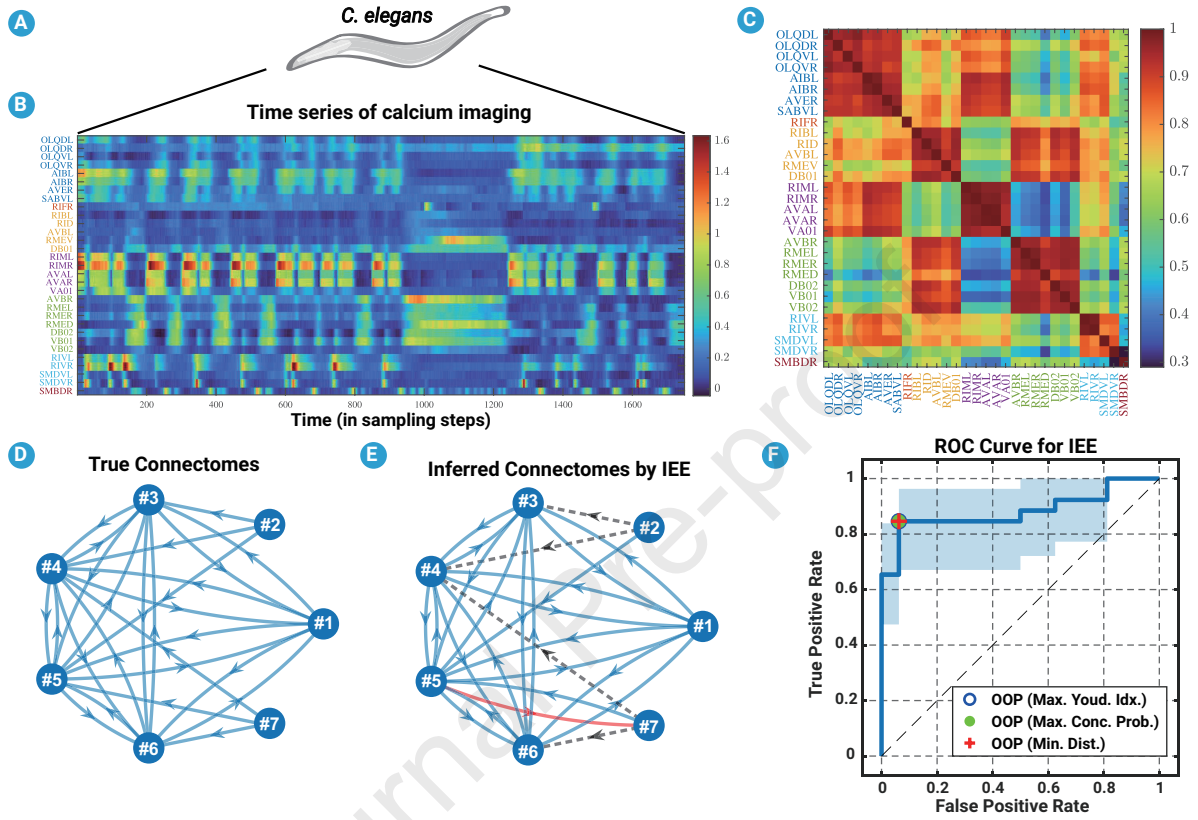


Figure 5. **Application of the IEE on inferring the neural connectomes of *C. elegans*** (A) is an illustration of *C. elegans*. (B) displays the calcium imaging time series of 31 key neurons, with their names listed on the left and colors representing different clusters. (C) is the cosine similarity matrix between neurons, aiding the clustering process. (D) is the true connectomes between 7 clusters, while (E) is the inferred causal network at the the optimal operating point (OOP) determined by IEE. The red edge represents a false positive, and the black dashed edges represent false negatives. (F) shows the ROC curve (the blue line) for IEE. The same OOP is obtained under three criteria, i.e. the maximum Youden index (the blue circle), the maximum concordance probability (the green dot), and the minimum distance to the point (0, 1) (the red cross). The shaded area around the ROC curve represents the 95% confidence interval obtained through bootstrapping. The AUC value of IEE is 0.882.

Table 2. Comparison of causal indices on the inference of *C. elegans* neural connectomes.

	Properties of ROC curves				Cosine Similarity	
	AUC	Maximum Youden index	Maximum concordance probability	Minimum distance to (0, 1)	to $\boldsymbol{C}$	to $\log(1+\boldsymbol{C})$
$\boldsymbol{C}^{\text{IEE}}$	**0.882**	**0.784**	**0.793**	**0.166**	**0.750**	**0.905**
$\boldsymbol{C}^{\text{GC}}$	0.858	0.721	0.740	0.198	0.430	0.678
$\boldsymbol{C}^{\text{TE}}$	0.796	0.620	0.656	0.269	0.477	0.726
$\boldsymbol{C}^{\text{CCM}}$	0.880	0.615	0.639	0.294	0.644	0.866

* The matrices $\boldsymbol{C}^{\text{IEE}}/\boldsymbol{C}^{\text{GC}}/\boldsymbol{C}^{\text{TE}}/\boldsymbol{C}^{\text{CCM}}$ represent the inferred connectomes by the four indices. The matrix $\boldsymbol{C}$ is the ground truth of neural connectomes. The best value in each column is shown in bold.

Journal Pre-proof

Application of IEE to COVID-19 transmission in Japan

We validated that IEE was a promising indicator for assessing the transmission dynamics of infectious diseases. Our study collected the daily confirmed COVID-19 cases from all 47 prefectures in Japan, spanning a duration of 1209 days from January 16, 2020 to May 8, 2023 (fig. S11).

First, we calculated the IEE indices for IntDC among different prefectures. IEE effectively ranked the influence across prefectures, with the top five affected areas by Tokyo being Kanagawa (with IEE value 0.601), Chiba (with IEE value 0.568), Saitama (with IEE value 0.534), Aichi (with IEE value 0.453), and Osaka (with IEE value 0.435). Remarkably, this ranking coincides with the geographical proximity and socio-economic connections to Tokyo. Kanagawa, Chiba and Saitama are in the same metropolitan area with Tokyo, while Aichi and Osaka are far from Tokyo but connected to Tokyo by expressway and Shinkansen.

Then, IEE was validated to coincide with the effective distance matrix D^{COVID} between prefectures. The $D^{\mathrm{COVID}} \in \mathbb{R}^{47\times 47}$ was non-symmetric and designed by incorporating factors such as geometric distances, human mobility, population sizes, and infectious rates across prefectures (based on the gravity model[53,54], see Supplementary Text and fig. S11 for details). The element D_{ij}^{COVID} served as a benchmark for quantifying COVID-19 transmission from prefecture i to j. The IEE values demonstrated a strong linear correlation with $\ln D^{\mathrm{COVID}}$, particularly when assessing the causality from Tokyo/Osaka to other prefectures (with Pearson correlation coefficients, i.e. PCCs, -0.906 for Tokyo and -0.860 for Osaka, Figs. **6**(A-B)). This correlation remained high for other regions (see fig. S12), such as Aichi (with PCC value -0.811), Hokkaido (with PCC value -0.751), Fukuoka (with PCC value -0.752), and Okinawa (with PCC value -0.811).

Further, IEE outperformed ConDC indices in practicality. Notably, the absolute value of the PCC between IEE and $\ln D^{\mathrm{COVID}}$ was 0.724 substantially higher than those obtained by GC 0.161, TE 0.284, and CCM 0.568 (average over specific prefecture, see the second to last column in Table **3** and the boxplot in Figure **6**(C)). More detailed comparisons to support the effectiveness of IEE were presented in Table **3** (with specific illustration for Tokyo in fig. S13).

IEE can also reflect asymmetry causal influence (i.e. effective distance) with high PCC under the IntDC framework, highlighting its advantage over ConDC methods. For example, the effective distance or IEE from Tokyo to Osaka ranks fifth (Figure **6**(A)), whereas the reverse direction from Osaka to Tokyo ranks second (Figure **6**(B)).

These results underscore the reliability and efficacy of IEE in providing quantitative insights into COVID-19 transmission dynamics in Japan. Importantly, IEE performs as a simple and valuable tool for causal analyses solely from daily confirmed time-series data, without the need for complex models considering various factors such as geodesic distances, human mobility, population sizes, and infectious rates.

Table 3. Comparison of IEE/GC/TE/CCM in measuring causal strengths in the transmission of COVID-19 data in Japan.

	$\lvert\mathrm{PCC}\left(c_{ij}^{\mathrm{Inf}}, \ln D_{ij}^{\mathrm{COVID}}\right)\rvert$ for specific prefecture (fixed i)							$\lvert\mathrm{PCC}\left(c_{ij}^{\mathrm{Inf}}, \ln D_{ij}^{\mathrm{COVID}}\right)\rvert$
	Tokyo (i = 13)	Osaka (i = 27)	Aichi (i = 23)	Hokkaido (i = 1)	Fukuoka (i = 40)	Okinawa (i = 47)	Average over all i	for all i, j with $i \neq j$
IEE	**0.906**	**0.860**	**0.811**	**0.751**	**0.752**	**0.811**	**0.724**	**0.748**
GC	0.462	0.387	0.236	0.070	0.125	0.164	0.161	0.166
TE	0.655	0.308	0.018	0.445	0.526	0.538	0.284	0.109
CCM	0.799	0.795	0.448	0.052	0.727	0.477	0.568	0.585

* i and j (ranging from 1 to 47) stand for different prefectures in Japan. c_{ij}^{Inf} is the causal strength from the prefecture i to j inferred by IEE, GC, TE, or CCM. D_{ij}^{COVID} is the effective distance between prefectures i and j. PCC is the Pearson correlation coefficient. The best value in each column is shown in bold.

Application of IEE to investigating circadian rhythms

We investigated the gene regulatory networks (GRNs) related to key genes on the circadian rhythm. The time series of gene expressions were measured by microarray from cultured rat cells[55,56]. Through decades of molecular and genetic studies, many key circadian genes, such as *Clock, Bmal1(Arntl), Dec1(Bhlhb2), Dec2(Bhlhb3), Cry1, Cry2, Per1, Per2, Per3*, have been identified on mammals[57,58]. Figure **6**(D) displayed the GRN around *Clock* at

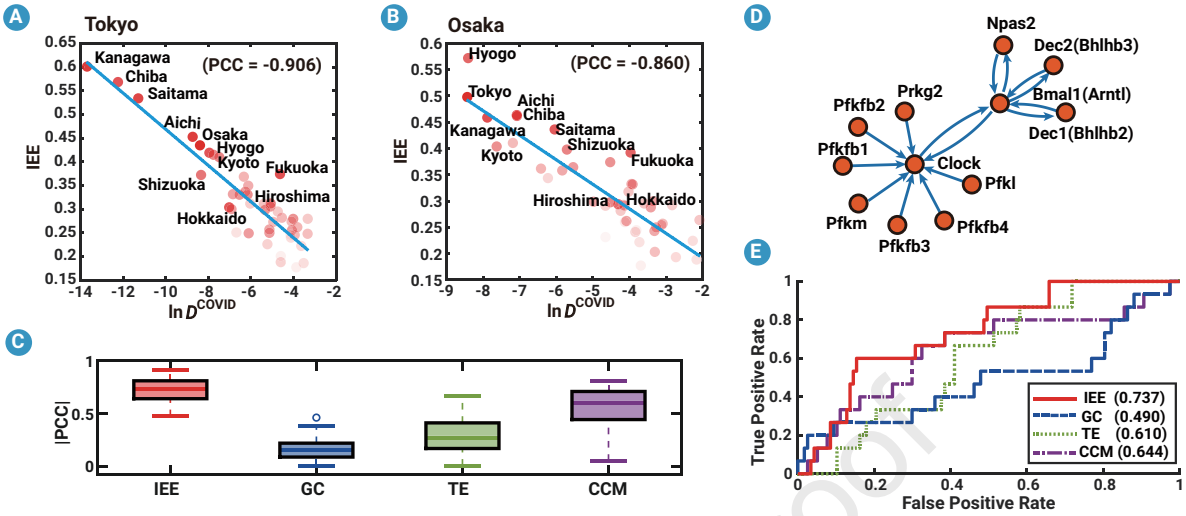


Figure 6. **Application of the IEE on the COVID-19 transmission in Japan and the gene regulatory network (GRN) of circadian rhythms** (A) shows that IEE values from Tokyo to other prefectures are highly linear-correlated with $\ln D^{\mathrm{COVID}}$, where D^{COVID} is the effective distance obtained from the gravity model in consideration of various factors. (B) is the result for IEE values from Osaka to the other prefectures. (C) is the boxplot for $|\mathrm{PCC}(c_{ij}^{\mathrm{Inf}}, \ln D_{ij}^{\mathrm{COVID}})|$ with average over fixed i, where PCC is the Pearson correlation coefficient and c^{Inf} is the inferred causal strengths by IEE, GC, TE, or CCM. The PCC linearity of IEE (0.724 ± 0.116) is significantly higher than that of GC (0.161 ± 0.099), TE(0.284 ± 0.168), and CCM (0.568 ± 0.174). (D) shows the GRN surrounding *Clock*, a key circadian gene. (E) demonstrates the ROC curves and AUC values of the IntDC index IEE, and three ConDC indices GC/TE/CCM.

the protein level, where the transcription factor *Clock* is phosphorylated by PFK family genes. We calculated the IEE/GC/TE/CCM to reconstruct the GRN (ROC curves and AUC values in Figure **6**(E)). IEE designed for quantifying IntDC presented a higher AUC value (0.737) than ConDC indices (0.490 for GC, 0.610 for TE, and 0.644 for CCM). We also tested the indices on the GRN surrounding Cry1/Cry2 (fig. S14), where IEE obtained the highest AUC value (0.639) and outperformed the others (0.428 for GC, 0.619 for TE, and 0.614 for CCM).

CONCLUDING REMARKS AND PERSPECTIVE

In summary, we have established a framework of IntDC based on dynamical systems theory and introduced the IEE criterion to quantify IntDC in this study. IEE measures the information flow between interventional causes and effects in the delay-embedding space, making it suitable for analyzing non-linear and non-separable systems[10,14,32]. Moreover, IEE is able to infer IntDC solely from observational time-series data, without requiring additional perturbations to the system. This property makes IEE particularly suitable for non-intervention systems. Both theoretical derivations and numerical examples presented in this study provide strong evidence to support the effectiveness, accuracy and robustness of IEE in detecting IntDC and reconstructing networks. Furthermore, IEE serves as an effective tool for evaluating and ranking the causal dependence between variables within a dynamical system. Through real-world examples, we illustrated the promising applicability of IEE in diverse fields such as regulatory inference and disease transmission studies.

Information-flow-based methods have been developing rapidly in recent years[33,34,36]. Liang's information flow theory, albeit with full nonlinearity in its theoretical formalism, is yet to be implemented for practical applications on real-world data. Existing implementations still rely on assumptions such as independent white noise and linearity when evaluating information flow from data. Our IEE algorithm, inspired by the conception information flow, is specifically designed to handle fully nonlinear systems and has demonstrated applicability across a variety of real datasets. The proposed IntDC framework, together with the IEE algorithm, advances the frontier of causality research by providing a practical and effective tool for nonlinear causal inference.

Runge et al.[46] summarized recent advances and key challenges in the field of causal inference and developed the platform https://causeme.net, which serves as a valuable resource for researchers. Causal inference holds great

promise for applications in earth system science and beyond. Our proposed IEE algorithm, together with the concept of IntDC, provides a novel and practical approach for investigating causality in complex nonlinear systems.

There are several important open issues that warrant further investigation and future development.

(1) The theory of IntDC and the IEE criterion can be extended to analyze causal relations between groups of variables. Specifically, in Eq. (2), the variables x and y can be generalized to multivariate vectors, enabling the investigation of complex interactions among multiple variables.

(2) The data used for computing IEE can be non-uniformly sampled in time. In this study, we employed the standard time-delayed embedding Eq. (3) and Eq. (4). However, according to the generalized Takens' embedding theorem, any set of $L + 1$ observations of x_t and y_t can construct topological diffeomorphisms to the manifolds $\mathcal{M}_X$ and $\mathcal{M}_Y$, respectively. As shown in Eq. (7), only the local neighborhood structure in the embedding space is essential for the computation. Therefore, the IEE algorithm can be naturally extended to infer causality from datasets sampled at varying or irregular time intervals.

(3) Although interventions in the admissible state space are allowed in Theorem 2, perturbations in the tangent space are sufficient to estimate IntDC. Under the stationarity assumption (A5) in Section 2.4, all trajectories with admissible initial points converge to the attractive manifold, and data on the attractor together with tangent-space perturbations are sufficient to quantify Eq. (6).

(4) To further distinguish direct and indirect causality, we can generalize IEE to its conditional version

$$\mathrm{cIEE}[x \to y|z] := \mathrm{CMI}(\delta \boldsymbol{X}_t, \delta \boldsymbol{Y}_{t+1} | \boldsymbol{Y}_{t+1}, \boldsymbol{Z}_t, \delta \boldsymbol{Z}_t), \tag{11}$$

where "cIEE" is short for the conditional IEE, z is a third variable whose time-delayed vector is $\boldsymbol{Z}_t$, and $\delta \boldsymbol{Z}_t$ represents the intervened deviation on $\boldsymbol{Z}_t$. Equation (11) measures the direct IntDC from x to y conditioned on z. Further, in combination with the well-known PC algorithm[59] or PCMCI[23], cIEE offers a feasible way to remove high-order indirect causal edges iteratively and reconstruct the direct causal network.

(5) Researchers have pointed out that time-delayed embedding algorithms are particularly suitable for deterministic dynamical systems with an attractive manifold[14,17,26]. However, the coupling strength between variables could influence the accuracy of these methods. Stark et al.[39] extended Takens' embedding to stochastic systems, providing a theoretical basis for applying embedding approaches beyond purely deterministic dynamics. In the Results section of this study, we demonstrated the effectiveness of IEE for Logistic systems with Gaussian noises. Nevertheless, how systematic factors, such as coupling strength and noise characteristics, affect the quantification of causal strength in more general settings remains an open question.

(6) We provide a concise introduction to the field of dynamical causality. The dynamical causality framework[10] summarized causal inference based on dynamical systems. Methods, such as GC[11], TE[13], CCM[14], and embedding entropy[10] are typical examples of dynamical causality approaches. Dynamical causality, or ConDC in this study, incorporates temporal ordering, allows feedback and causal loops, and quantifies causal strength — representing an advance over statistical causal inference. IntDC in this study further extended this framework by introducing interventions, and IEE provides an efficient algorithm for quantifying IntDC in non-intervention complex systems.

(7) One limitation of IEE is its requirement for long time-series data, typically over 100 time points. Some datasets, such as spatial transcriptomes[60], contain many samples along the spatial dimension but few time points. A potential approach to address this limitation is to assign pseudo-time labels to these samples[61,62]. By converting the data into a time-series format, it may become possible to infer causal relationships between variables. This represents an important direction for future work.

(8) Moreover, causal inference empowered by deep learning is emerging as a frontier in research. Notable advances include CausalEGM[63], Causalformer[64], intervened reservoir computing[65], and reservoir cross mapping[66]. In the authors' view, AI and logistic-based causal inference methods have distinct advantages. Logistic-based methods are more interpretable and provide mechanistic insights, while AI methods are highly efficient at discovering complex correlations or mappings between different parts of a complex system. However, these approaches are also complementary: combining AI with logistic-based method should provide a more comprehensive understanding of complex systems. Integrating the IntDC framework with neural networks presents a promising direction for further exploration. On one hand, causality theory provides interpretability to artificial intelligence; on the other hand, large AI foundation models offer unprecedented capacity to uncover causal relationships in complex data . These developments signal the advent of a transformative "big causality era", in which data-driven discovery and causal reasoning evolve in synergy.

Journal Pre-proof

RESOURCES AVAILABILITY

Data and code availability

The code for IEE is available at https://github.com/smsxiaomayi/IEE.

FUNDING AND ACKNOWLEDGMENTS

This work was supported by the National Natural Science Foundation of China [grant numbers 42450192, 12301620, 42450135, 11925103, 32100509, T2350003, 12131020, 42450084, 12326614, 12426310, 12531018, and 42525604], the Shanghai Municipal Data Bureau special fund for urban digital transformation [grant number 202401065], the AI for Science Foundation of Fudan University [grant number FudanX24AI041], the Lingang Laboratory [grant number LGL-1987-06], the AI for Science Program of Shanghai Municipal Education Commission [grant numbers 24RGZN10, 23JS1401300], National Key R&D Program of China [grant numbers 2025YFC3409300, 2025YFF1207900, 2022YFA1004800, and 2025YFA1016500], Zhejiang Province Vanguard Goose-Leading Initiative [grant number 2025C01114], Shenzhen Medical Research Fund [grant number E250200621], the Japan Science and Technology Agency Moonshot R&D [grant number JPMJMS2021], the Institute of AI and Beyond of UTokyo, the International Research Center for Neurointelligence (WPI-IRCN) at The University of Tokyo Institutes for Advanced Study (UTIAS), and the Cross-ministerial Strategic Innovation Promotion Program (SIP), the 3rd period of SIP [grant number JPJ012207].

AUTHOR CONTRIBUTIONS

J.S. contributed to the conceptualization, methodology, investigation, computation, data analysis, visualization, and writing the original draft. Y.L. contributed to the investigation, computation, data analysis, visualization, and writing the original draft. J.Z. contributed to the investigation, computation, data analysis, and visualization, and writing the original draft. S.L. contributed to the investigation, computation, data analysis, and visualization. R.B. contributed to the investigation, and data analysis. K.A. contributed to the conceptualization, investigation, and supervision. L.C. contributed to the conceptualization, investigation, and supervision. W.L. contributed to the conceptualization, investigation, and supervision. All authors contributed to the manuscript and approved the final version.

DECLARATION OF INTERESTS

The authors declare no conflicts of interest.

SUPPLEMENTAL INFORMATION

It can be found online at XXX(DOI).

Journal Pre-proof

Journal Pre-proof

REFERENCES

[1] Jerzy S Neyman. On the application of probability theory to agricultural experiments. Essay on principles. Section 9. *Stat. Sci*., 5(4):465–472, 1990.

[2] Donald B Rubin. Bayesian inference for causal effects: The role of randomization. *The Ann. Stat*., 6(1):34–58, 1978.

[3] Jasjeet S Sekhon. The Neyman-Rubin model of causal inference and estimation via matching methods. *The Oxf. Handb. Political Methodol*., 2:1–32, 2008.

[4] Sewall Wright. Correlation and causation. *J. Agric. Res*., 20:557–585, 1921.

[5] Sewall Wright. The method of path coefficients. *The Ann. Math. Stat*., 5(3):161–215, 1934.

[6] Judea Pearl. Causal diagrams for empirical research. *Biometrika*, 82(4):669–688, 1995.

[7] Judea Pearl. Causal inference in statistics: An overview. *Stat. Surv*., 3:96–146, 2009.

[8] Judea Pearl. *Causality: models, reasoning, and inference*. Cambridge University Press, UK, 2000.

[9] Joshua D Angrist, Guido W Imbens, and Donald B Rubin. Identification of causal effects using instrumental variables. *J. Am. Stat. Assoc*., 91(434):444–455, 1996.

[10] Jifan Shi, Luonan Chen, and Kazuyuki Aihara. Embedding entropy: a nonlinear measure of dynamical causality. *J. R. Soc. Interface*, 19(188):20210766, 2022.

[11] Clive W J Granger. Investigating causal relations by econometric models and cross-spectral methods. *Econometrica*, 37(3):424–438, 1969.

[12] Bethany Lusch, Pedro D Maia, and J Nathan Kutz. Inferring connectivity in networked dynamical systems: Challenges using granger causality. *Phys. Rev. E*, 94(3):032220, 2016.

[13] Thomas Schreiber. Measuring information transfer. *Phys. Rev. Lett*., 85(2):461, 2000.

[14] George Sugihara, Robert May, Hao Ye, Chih-hao Hsieh, Ethan Deyle, Michael Fogarty, and Stephan Munch. Detecting causality in complex ecosystems. *Science*, 338(6106):496–500, 2012.

[15] Siyang Leng, Huanfei Ma, Jürgen Kurths, Ying-Cheng Lai, Wei Lin, Kazuyuki Aihara, and Luonan Chen. Partial cross mapping eliminates indirect causal influences. *Nat. Commun*., 11(1):1–9, 2020.

[16] Xiong Ying, Si-Yang Leng, Huan-Fei Ma, Qing Nie, Ying-Cheng Lai, and Wei Lin. Continuity scaling: A rigorous framework for detecting and quantifying causality accurately. *Research*, 2022:9870149, 2022.

[17] Hao Ye, Ethan R Deyle, Luis J Gilarranz, and George Sugihara. Distinguishing time-delayed causal interactions using convergent cross mapping. *Sci. Rep*., 5(1):14750, 2015.

[18] Louis M Pecora, Thomas L Carroll, and James F Heagy. Statistics for mathematical properties of maps between time series embeddings. *Phys. Rev. E*, 52(4):3420, 1995.

[19] Daniel Harnack, Erik Laminski, Maik Schünemann, and Klaus Richard Pawelzik. Topological causality in dynamical systems. *Phys. Rev. Lett*., 119(9):098301, 2017.

[20] José M Amigó and Yoshito Hirata. Detecting directional couplings from multivariate flows by the joint distance distribution. *Chaos: An Interdiscip. J. Nonlinear Sci*., 28(7):075302, 2018.

[21] Stavros K Stavroglou, Athanasios A Pantelous, H Eugene Stanley, and Konstantin M Zuev. Unveiling causal interactions in complex systems. *Proc. Natl. Acad. Sci. U.S.A.*, 117(14):7599–7605, 2020.

[22] Peng Tao, Qifan Wang, Jifan Shi, Xiaohu Hao, Xiaoping Liu, Bin Min, Yiheng Zhang, Chenyang Li, He Cui, and Luonan Chen. Detecting dynamical causality by intersection cardinal concavity. *Fundam. Res*., 2023.

[23] Jakob Runge, Peer Nowack, Marlene Kretschmer, Seth Flaxman, and Dino Sejdinovic. Detecting and quantifying causal associations in large nonlinear time series datasets. *Sci. Adv*., 5(11):eaau4996, 2019.

[24] Karl J Friston, Lee Harrison, and Will Penny. Dynamic causal modelling. *Neuroimage*, 19(4):1273–1302, 2003.

[25] Klaas E Stephan, Lee M Harrison, Stefan J Kiebel, Olivier David, Will D Penny, and Karl J Friston. Dynamic causal models of neural system dynamics: current state and future extensions. *J. Biosci*., 32(1):129–144, 2007.

[26] Anna Krakovská, Jozef Jakubík, Martina Chvosteková, David Coufal, Nikola Jajcay, and Milan Paluš. Comparison of six methods for the detection of causality in a bivariate time series. *Phys. Rev. E*, 97(4):042207, 2018.

[27] George Stepaniants, Bingni W Brunton, and J Nathan Kutz. Inferring causal networks of dynamical systems through transient dynamics and perturbation. *Phys. Rev. E*, 102(4):042309, 2020.

[28] Dmitry A Smirnov. Quantification of causal couplings via dynamical effects: A unifying perspective. *Phys. Rev. E*, 90(6):062921, 2014.

[29] Dmitry A Smirnov. Transfer entropies within dynamical effects framework. *Phys. Rev. E*, 102(6):062139, 2020.

[30] X San Liang and Richard Kleeman. Information transfer between dynamical system components. *Phys. Rev. Lett*., 95(24):244101, 2005.

[31] X San Liang. Unraveling the cause-effect relation between time series. *Phys. Rev. E*, 90(5):052150, 2014.

[32] X San Liang. Information flow and causality as rigorous notions ab initio. *Phys. Rev. E*, 94(5):052201, 2016.

[33] X San Liang. Normalized multivariate time series causality analysis and causal graph reconstruction. *Entropy*, 23(6):679, 2021.

[34] Dionissios T Hristopulos. Information flow rate for cross-correlated stochastic processes. *IEEE Trans. on Signal Process*., 72:839–854, 2024.

[35] Bin Yi and Sougato Bose. Quantum liang information flow as causation quantifier. *Phys. Rev. Lett*., 129(2):020501, 2022.

[36] Carlos A Pires, David Docquier, and Stéphane Vannitsem. A general theory to estimate information transfer in nonlinear systems. *Physica D: Nonlinear Phenom*., 458:133988, 2024.

[37] Floris Takens. Detecting strange attractors in turbulence. In *Dynamical systems and turbulence, Warwick 1980*, pages 366–381. Springer, 1981.

[38] Tim Sauer, James A Yorke, and Martin Casdagli. Embedology. *J. Stat. Phys*., 65:579–616, 1991.

[39] Jaroslav Stark, DS Broomhead, ME Davies, and J Huke. Takens embedding theorems for forced and stochastic systems. *Nonlinear Anal. Theory, Methods Appl*., 30(8):5303–5314, 1997.

[40] Bree Cummins, Tomás Gedeon, and Kelly Spendlove. On the efficacy of state space reconstruction methods in determining causality. *SIAM J. on Appl. Dyn. Syst*., 14(1):335–381, 2015.

Journal Pre-proof

[41] Naomi Altman and Martin Krzywinski. Points of significance: Association, correlation and causation. *Nat. Methods*, 12(10), 2015.

[42] Ali Shojaie and Emily B Fox. Granger causality: A review and recent advances. *Annu. Rev. Stat. Its Appl.*, 9:289–319, 2022.

[43] Kevin B Korb, Lucas R Hope, Ann E Nicholson, and Karl Axnick. Varieties of causal intervention. In *PRICAI 2004: Trends in Artificial Intelligence*, pages 322–331. Springer, 2004.

[44] Pierre-Olivier Amblard and Olivier JJ Michel. The relation between granger causality and directed information theory: A review. *Entropy*, 15(1):113–143, 2012.

[45] Thomas M Cover. *Elements of information theory*. John Wiley & Sons, 1999.

[46] Jakob Runge, Sebastian Bathiany, Erik Bollt, Gustau Camps-Valls, Dim Coumou, Ethan Deyle, Clark Glymour, Marlene Kretschmer, Miguel D Mahecha, Jordi Muñoz-Marí, et al. Inferring causation from time series in earth system sciences. *Nat. Commun.*, 10(1):2553, 2019.

[47] Kazuyuki Aihara, T Takabe, and Masashi Toyoda. Chaotic neural networks. *Phys. Lett. A*, 144(6-7):333–340, 1990.

[48] Masaharu Adachi and Kazuyuki Aihara. Associative dynamics in a chaotic neural network. *Neural Networks*, 10(1):83–98, 1997.

[49] Steven J. Cook, Travis A. Jarrell, Christopher A. Brittin, Yi Wang, Adam E. Bloniarz, Maksim A. Yakovlev, Ken C. Q. Nguyen, Leo T.-H. Tang, Emily A. Bayer, Janet S. Duerr, Hannes E. Bülow, Oliver Hobert, , David H. Hall, and Scott W. Emmons. Whole-animal connectomes of both *Caenorhabditis elegans* sexes. *Nature*, 571:63–71, 2019.

[50] Saul Kato, Harris S. Kaplan, Tina Schrödel, Susanne Skora, Theodore H. Lindsay, Eviatar Yemini, Shawn Lockery, and Manuel Zimmer. Global brain dynamics embed the motor command sequence of *Caenorhabditis elegans*. *Cell*, 163(3):656–669, 2015.

[51] Amitava Banerjee, Sarthak Chandra, and Edward Ott. Network inference from short, noisy, low time-resolution, partial measurements: Application to *C. elegans* neuronal calcium dynamics. *Proc. Natl. Acad. Sci. U.S.A.*, 120(12):e2216030120, 2023.

[52] Emmons Lab. Hermaphrodite and Male Connectomes (Adjacency Matrices), Adults (corrected July 2020). available at `https://wormwiring.org/pages/adjacency.html`, 2020. accessed: 2023-12-15.

[53] Hugo Barbosa, Marc Barthelemy, Gourab Ghoshal, Charlotte R. James, Maxime Lenormand, Thomas Louail, Ronaldo Menezes, José J. Ramasco, Filippo Simini, and Marcello Tomasini. Human mobility: Models and applications. *Phys. Rep.*, 734:1–74, 2018.

[54] George Kingsley Zipf. The $p_1 p_2/d$ hypothesis: On the intercity movement of persons. *Am. Sociol. Rev.*, 11(6):677–686, 1946.

[55] Yong Wang, Xiang-Sun Zhang, and Luonan Chen. A network biology study on circadian rhythm by integrating various omics data. *OMICS*, 13(4):313–324, 2009.

[56] Soshi Kawaguchi, Atsuki Shinozaki, Masuo Obinata, Kaoru Saigo, Yoshiyuki Sakaki, and Hajime Tei. Establishment of cell lines derived from the rat suprachiasmatic nucleus. *Biochem. Biophys. Res. Commun.*, 355(2):555–561, 2007.

[57] Caroline H Ko and Joseph S Takahashi. Molecular components of the mammalian circadian clock. *Hum. Mol. Genet.*, 15(suppl_2):R271–R277, 2006.

[58] Hiroki R Ueda, Satoko Hayashi, Wenbin Chen, Motoaki Sano, Masayuki Machida, Yasufumi Shigeyoshi, Masamitsu Iino, and Seiichi Hashimoto. System-level identification of transcriptional circuits underlying mammalian circadian clocks. *Nat. Genet.*, 37(2):187–192, 2005.

[59] Peter Spirtes and Clark Glymour. An algorithm for fast recovery of sparse causal graphs. *Soc. Sci. Comput. Rev.*, 9(1):62–72, 1991.

[60] Lambda Moses and Lior Pachter. Museum of spatial transcriptomics. *Nat. Methods*, 19(5):534–546, 2022.

[61] Cole Trapnell, Davide Cacchiarelli, Jonna Grimsby, Prapti Pokharel, Shuqiang Li, Michael Morse, Niall J Lennon, Kenneth J Livak, Tarjei S Mikkelsen, and John L Rinn. The dynamics and regulators of cell fate decisions are revealed by pseudotemporal ordering of single cells. *Nat. Biotechnol.*, 32(4):381–386, 2014.

[62] Jifan Shi, Tiejun Li, Luonan Chen, and Kazuyuki Aihara. Quantifying pluripotency landscape of cell differentiation from scRNA-seq data by continuous birth-death process. *PLoS Comput. Biol.*, 15(11):e1007488, 2019.

[63] Qiao Liu, Zhongren Chen, and Wing Hung Wong. CausalEGM: a general causal inference framework by encoding generative modeling. *arXiv preprint arXiv:2212.05925*, 2022.

[64] Ziyu Lu, Anika Tabassum, Shruti Kulkarni, Lu Mi, J Nathan Kutz, Eric Shea-Brown, and Seung-Hwan Lim. Attention for causal relationship discovery from biological neural dynamics. *arXiv preprint arXiv:2311.06928*, 2023.

[65] Jintong Zhao, Zhongxue Gan, Ruixi Huang, Chun Guan, Jifan Shi, and Siyang Leng. Detecting dynamical causality via intervened reservoir computing. *Commun. Phys.*, 7(1):232, 2024.

[66] Ren Cao, Jintong Zhao, Chun Guan, Huanfei Ma, Jifan Shi, and Siyang Leng. Reservoir cross mapping as a nonlinear framework for detecting dynamical causality. *Cell Rep. Phys. Sci.*, 6(7):102683, 2025.

Journal Pre-proof

Journal Pre-proof

A

Unknown System $\mathcal{O} = \{(x_t, y_t, z_t)|t \in \mathbb{N}\}$

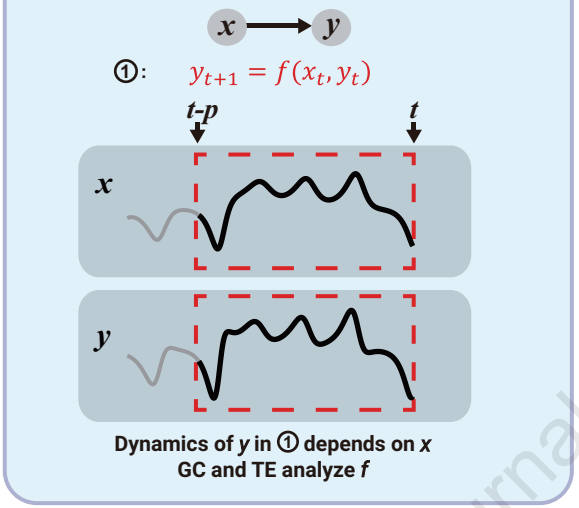
Observation (x_t, y_t)

Observation (x_t, y_t)

B

Constructive Dynamical Causality (ConDC)

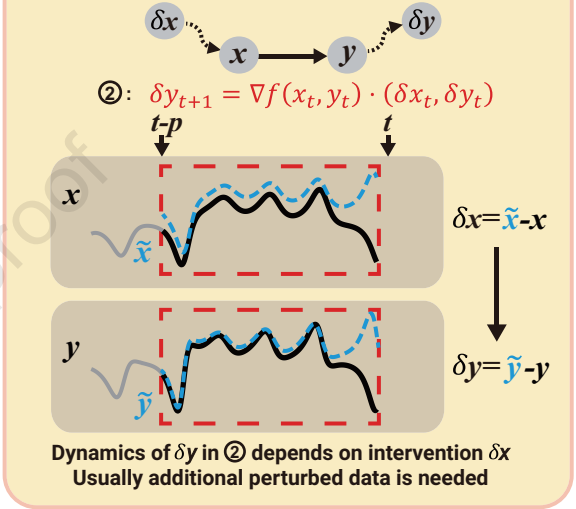
ConDC in original time-series space



C

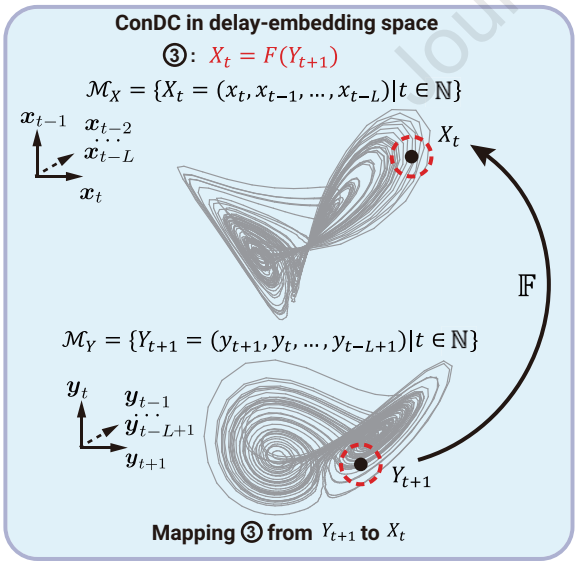
Interventional Dynamical Causality (IntDC)

IntDC in original time-series space



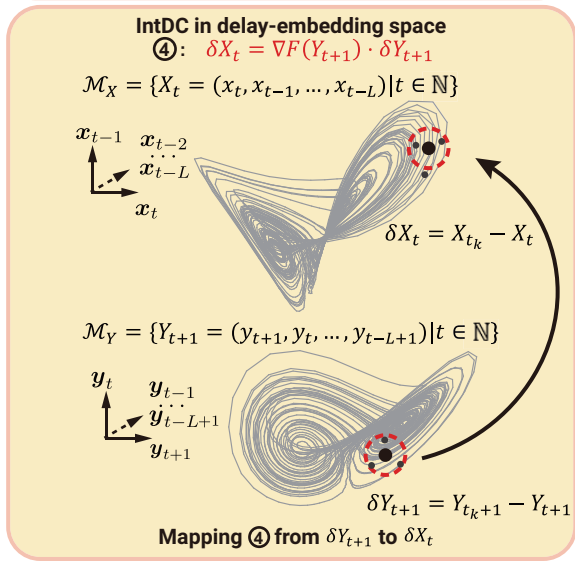
D

ConDC in delay-embedding space



E

IntDC in delay-embedding space

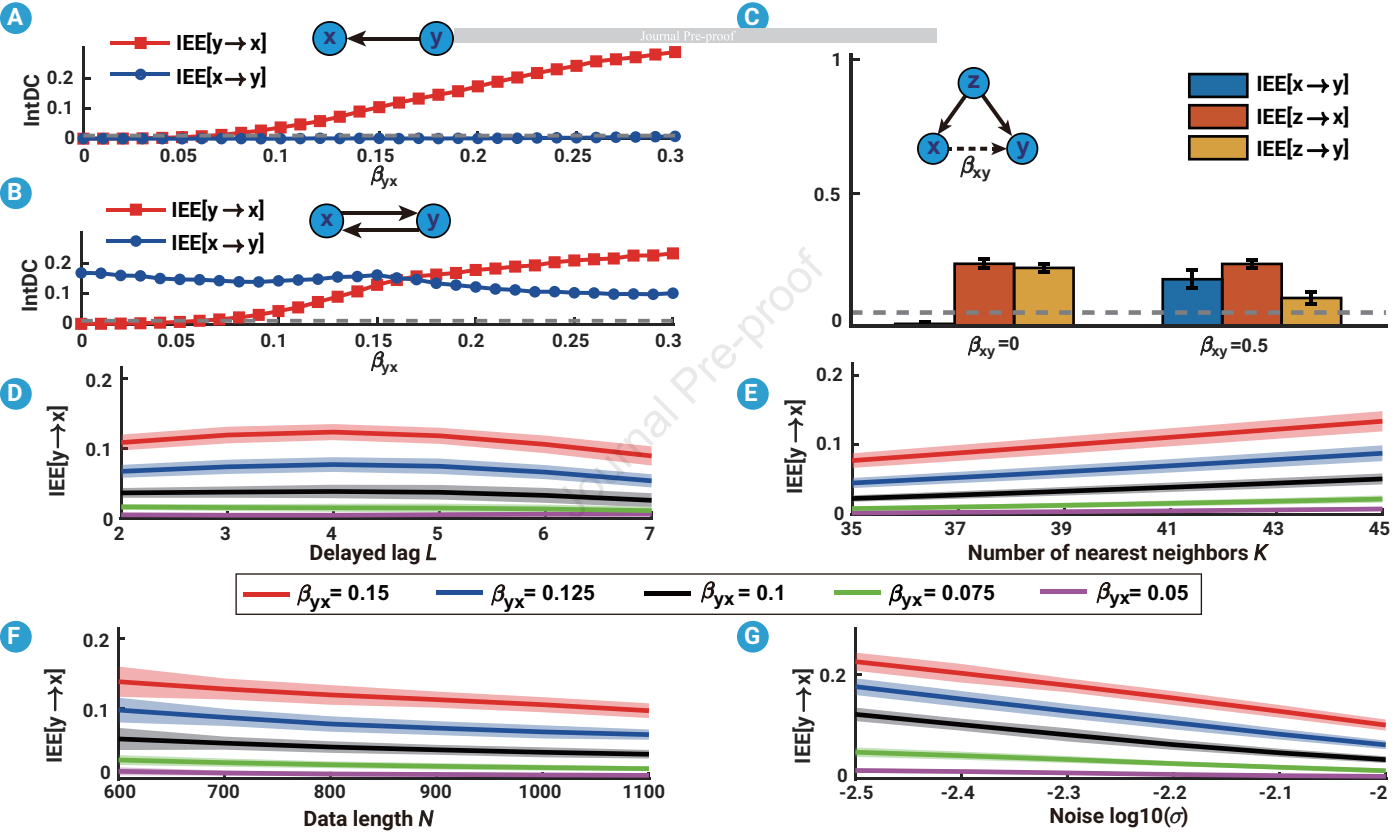


F

Interventional Embedding Entropy (IEE)

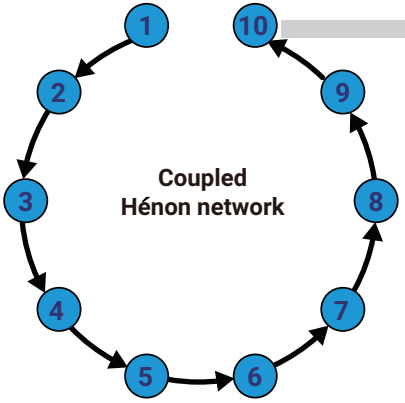
$$\mathrm{IEE}[x \to y] = \mathrm{CMI}(\delta X_t, \delta Y_{t+1} | Y_{t+1})$$

Journal Pre-proof

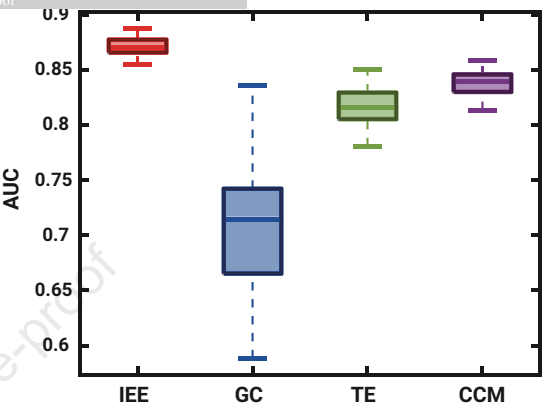


Journal Pre-proof

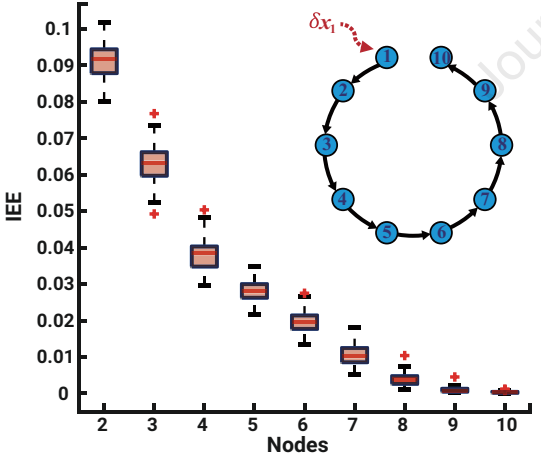
A



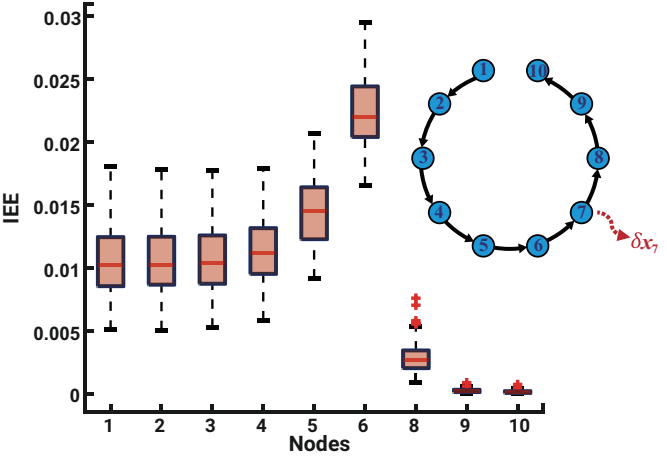
B



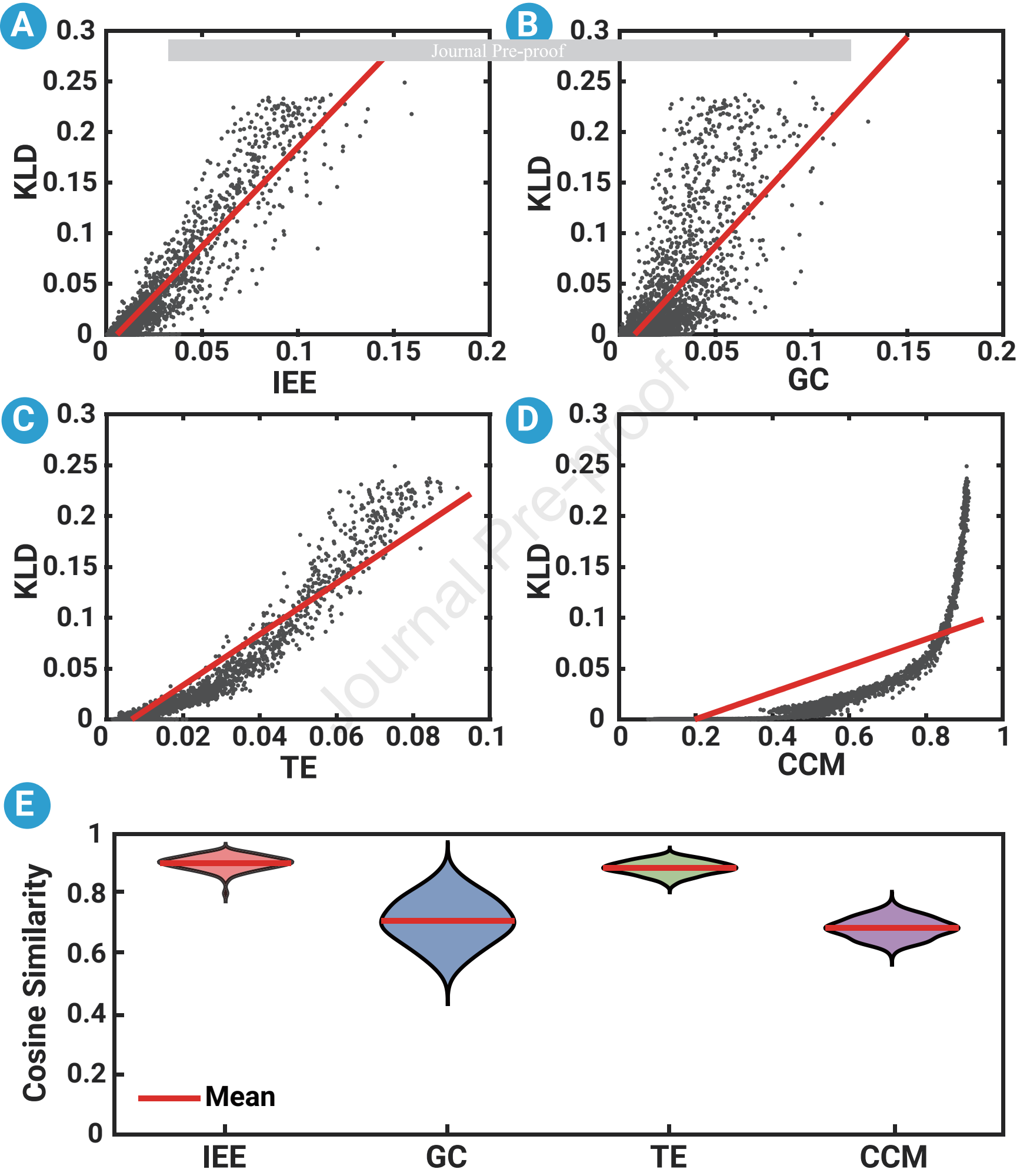
C



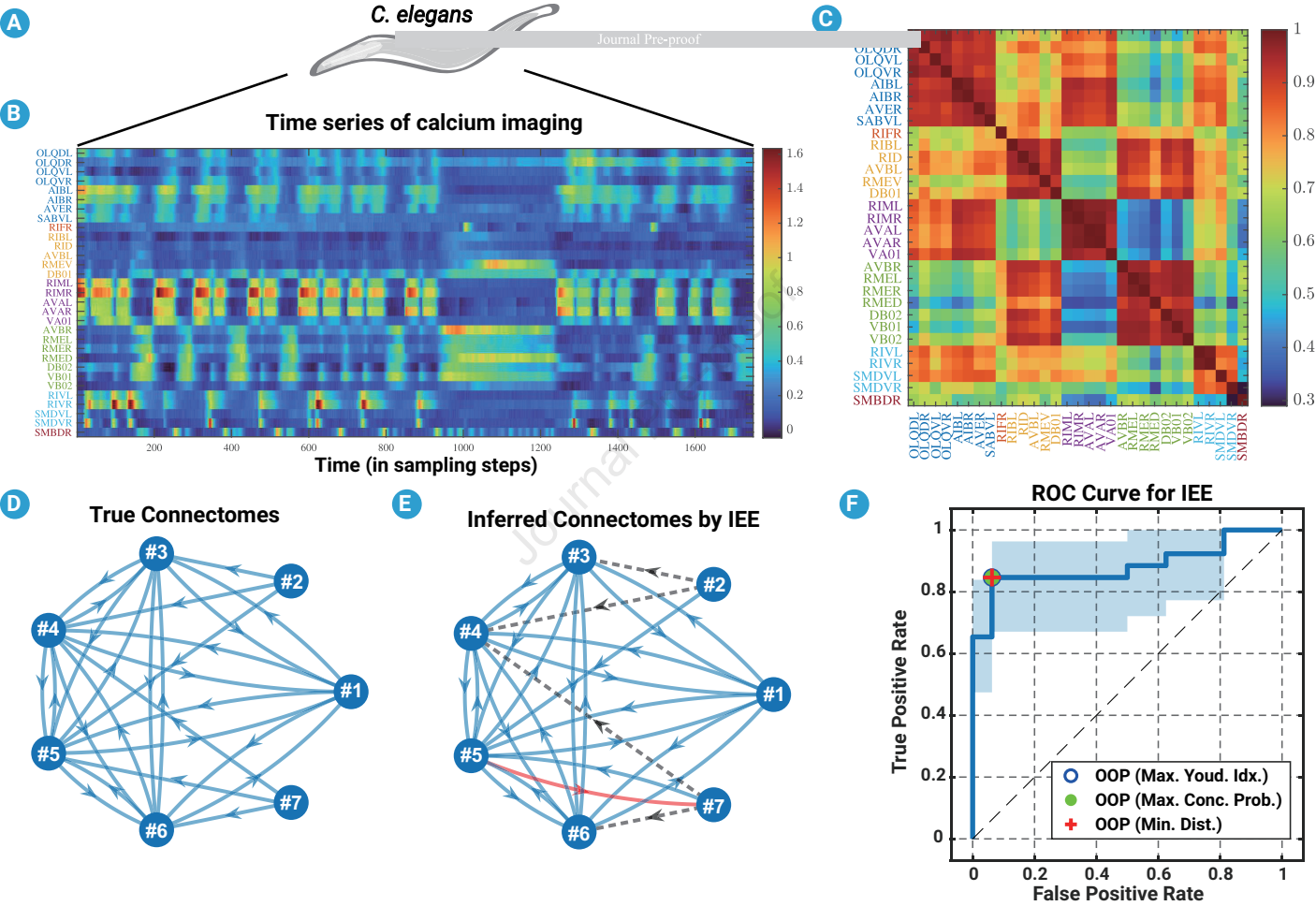
D

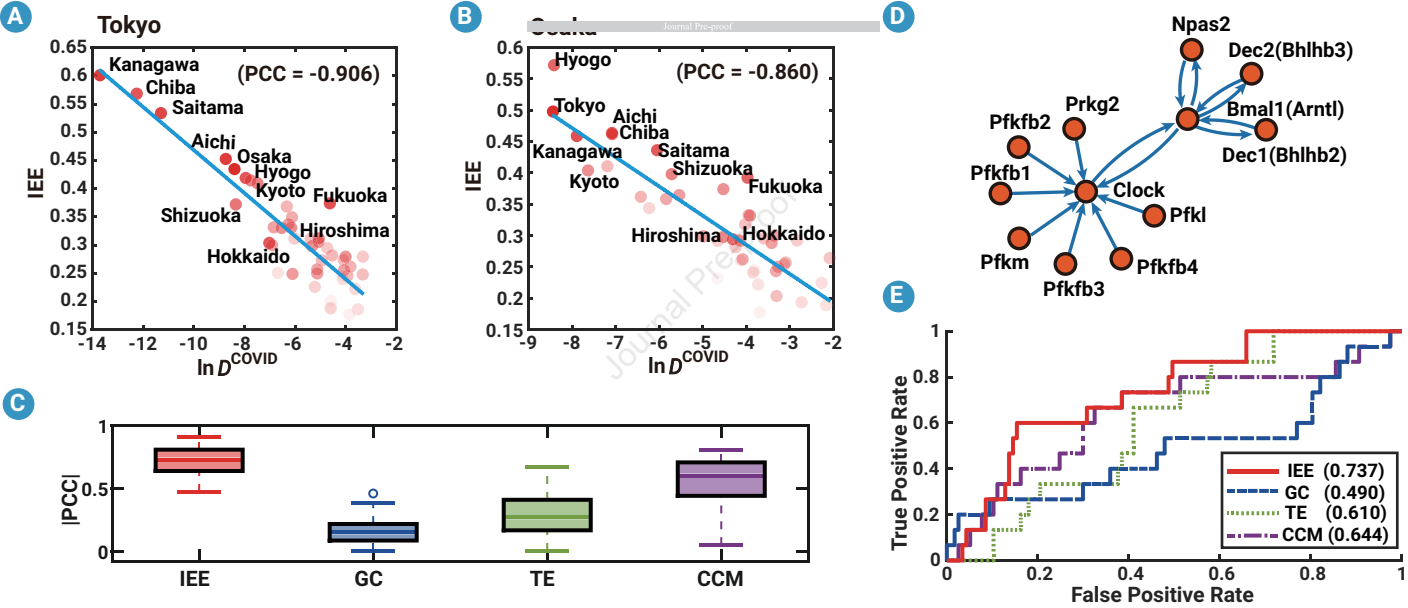


Journal Pre-proof



Journal Pre-proof





Journal Pre-proof

Public Summaries

- A theoretical framework for interventional dynamical causality is proposed.
- Dynamical systems theory is integrated with modern causal inference.
- The interventional embedding entropy (IEE) method quantifies causal strength directly from observational data.
- The IEE approach enables robust and effective causal detection across diverse non-intervention complex systems.

Journal Pre-proof